Geotextiles and Geomembranes xxx (xxxx) xxx

Contents lists available at ScienceDirect

Geotextiles and Geomembranes

journal homepage: www.elsevier.com/locate/geotexmem

Regular Paper

Long-term durability of two HDPE geomembranes formulated with polyethylene of raised temperature resistance (PE-RT)

Matthew Clinton [a], R. Kerry Rowe [b,*]

[a] GeoEngineering Centre at Queen's-RMC, Queen's University, Kingston, ON, K7L 3N6, Canada
[b] Geotechnical and Geoenvironmental Engineering, GeoEngineering Centre at Queen's-RMC, Queen's University, Ellis Hall, Kingston, ON, K7L 3N6, Canada

ARTICLE INFO

Keywords:
Geosynthetics
Geomembrane
Durability
High temperature
PE-RT
Stress crack resistance

ABSTRACT

The performance of four 1.5-mm HDPE geomembranes from the same manufacturer each with a different resin and additive package is examined in a synthetic municipal solid waste leachate at five temperatures (40, 65, 75, 85, 95 °C) for 7.5 years. Two geomembranes used polyethylene with raised temperature resistance (PE-RT) resins and two used more conventional polyethylene resins. All four geomembranes were inferred to contain hindered amines stabilizers (HAS) and had very high off-the-roll stress crack resistance (SCR_o) values that decreased to stable, more representative SCR_m values shortly after immersion and it was found that the 3-stage GMB degradation model applied to both Std-OIT and HP-OIT. The time to nominal failure is predicted for a range of temperatures using Arrhenius modelling and the representative SCR_m values. Despite the fact that all four GMBs had similar times to nominal failure at constant elevated temperatures (65–95 °C), it is shown that the HAS used in one of the PE-RT GMBs served a useful function in extending its life in situations such as elevated temperature landfills where there is a time-temperature history to be accommodated by the GMB. The value of considering both Std- and HP-OIT is also demonstrated.

1. Introduction

Much research has been conducted into the use of high-density polyethylene (HDPE) geomembranes (GMBs), including extensive recent work (e.g., Touze 2020; Morsy et al., 2021; Rowe, 2020; McWatters et al. 2020; Morsy and Rowe, 2020; Abdelaal et al., 2019; Marcotte and Fleming, 2019; Eldesouky and Brachman, 2018; Giroud 2016; Rowe 2011; Rowe and Islam 2009; Tognon et al., 1999). However, there remains a paucity of research into the long-term performance of so-called "high temperature" HDPE GMB products made from polyethylene of raised temperature resistance (PE-RT) resins.

PE-RT is a class of polyethylene (PE) resin developed for elevated temperature applications, most notably in the plastic pipe industry (recognized in ISO 1043-1, 1997 and ASTM, 2014) where they are an alternative to cross-linked polyethylene (PEX) for hot fluid conveyance owing to their improved flexibility and processability over PEX (Damen et al., 2001; Montes et al., 2012). Compared to traditional ethylene-α-olefin based PE resins, PE-RT resins optimize tie chain concentration through the introduction of certain co-monomers during polymerization (e.g., octane, hexane) resulting in side groups (e.g., hexyl side chain) that cannot fit into the linear crystal lamellae structure and are pushed out (Damen et al., 2001). This imperfection, in turn, increases the probability of tie-chain formation compared to more linear PE and can result in improved mechanical properties at elevated temperatures (Damen et al., 2001). Commercial examples include Dowlex 2344 (ethylene-octene co-polymer), Dowlex 2377, Intrepid 2499 and Total XRT70. It is these tie-chains in addition to the chain entanglements that constitute the interlamellar connections in the amorphous zone of semi-crystalline PE. Most studies on PE-RT have focused on their application in pressurized plastic pipe (e.g., Damen et al., 2001; Redhead et al., 2012; Montes et al., 2012) and some jurisdictions have even set minimum specifications for such pipes (e.g., Germany DIN, 2001). Accordingly, most archival studies on PE-RT grade resins were based on the long-term hydrostatic strength test (e.g., ASTM, 2013a) which pressurizes a segment of plastic pipe at elevated temperature to accelerate slow crack growth (SCG), which is the typical failure mechanism for pressurized plastic pipe (Redhead et al., 2012).

Geomembranes (GMBs) are widely used as hydraulic barriers and have service lives ranging from decades to many centuries in a variety of applications (e.g., Rowe et al., 2014; Abdelaal et al., 2014; Ewais et al.

* Corresponding author.
E-mail addresses: m.clinton@queensu.ca (M. Clinton), kerry.rowe@queensu.ca (R.K. Rowe).

https://doi.org/10.1016/j.geotexmem.2023.11.003
Received 19 July 2023; Received in revised form 5 November 2023; Accepted 25 November 2023
Available online 18 December 2023

2014; Rowe et al., 2020). Some of the factors that affect GMB service life include the GMB itself (resin and additive package), its chemical interaction with the leachate, how it was designed and installed (e.g., induced tensile strains) and the liner temperature (Rowe, 2020). Increasingly, GMBs are being used in hot applications (e.g., bio heap leaching, solar brine ponds, hot industrial effluents etc.). Even some landfill practices can generate very high temperatures on the bottom liner (e.g., bio-reactor landfills with leachate re-circulation; aluminum co-disposal etc.). Jafari et al. (2014) found that even relatively short periods of increased temperature in landfills can substantially reduce the GMB's service life. In solar brine and geothermal ponds, which represent some of the hottest geomembrane applications, liner temperatures exceeding 80 °C have been reported (Scheirs, 2009; Leblanc et al., 2011). Thus, there is an interest in GMBs with increased durability at these temperatures.

1.1. Geomembrane service-life and degradation model

Based on laboratory ageing studies involving fluid immersion, the thermo-oxidative degradation of PE GMB typically occurs in three stages (Ewais and Rowe, 2014; Hsuan and Koerner, 1998). Stage I involves the depletion of antioxidants and stabilizers (AO-S) which are added to prolong the onset of oxidative degradation. Stage II is a lag period where although the mobile AO-S have depleted, there are no changes detected in the mechanical properties. Stage III starts when the mechanical properties begin to degrade (e.g., tensile break strength). The time to nominal failure (t_{NF}), which marks the end of Stage III, is often defined as the time until a mechanical property degrades to 50% of its (a) initial tensile elongation or strength at break (e.g., Hsuan and Koerner, 1998), or (b) representative stress crack resistance (SCR_m to be discussed later; Rowe et al., 2019), or (c) some specified value (e.g., by GRI-GM13 (2021); Morsy and Rowe 2020). The depletion of AO-S (Stage I) typically occurs through two mechanisms: (1) chemical consumption: either related to their intended function or by transformation/de-activation into other compounds and, more critically; (2) physical loss due to extraction when the GMB is in contact with a fluid (Clinton and Rowe, 2023; Rimal and Rowe 2009; Scheirs, 2009). The length of Stage I (AO-S depletion) can be assessed by monitoring the change in oxidative induction time (OIT) with ageing time and there are two relevant tests: Standard (Std-OIT) and high-pressure (HP-OIT). Since both tests detect different parts of the AO-S package (which deplete differently), there can often be two different lengths/types of Stage I depending on which

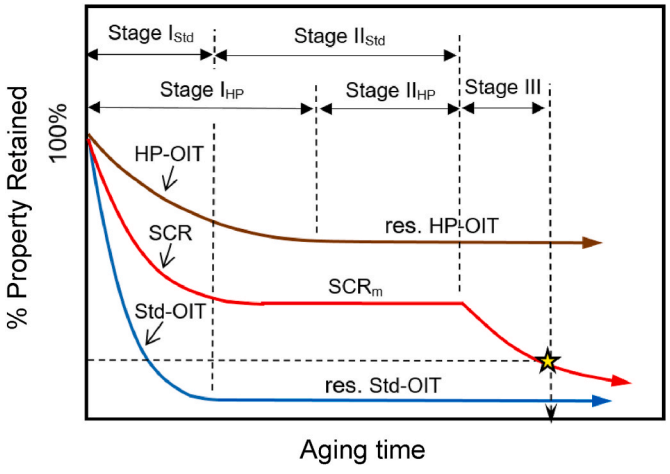

Fig. 1. Three-stage degradation model based on Std-OIT, HP-OIT and SCR for a leachate-immersed HDPE GMB containing HAS. The initial drop in SCR to a stable value (SCR_m) is typical for HDPE GMBs with high off-the-roll SCR but is not degradation. Mechanical degradation begins when SCR departs this plateau.

OIT test is used and, consequently, two different lengths of Stage II (Fig. 1). t_{NF} represents the GMB's nominal "resistance" to aging. Service life is related to the t_{NF} but may be greater than or less than t_{NF} depending on the "demand" placed on the GMB (i.e., how it was installed/welded, the magnitude of induced strains and how the facility is operated).

The length of Stage I will depend primarily on the types and amounts of AO-S used and their interaction with the contained fluid and, to a lesser degree, on the resin (Morsy et al., 2021; Scheirs, 2009). Since the added phosphite stabilizers are generally only effective in the melt processing range (150–300 °C), the AO-S that usually contribute to GMB longevity at end-use temperatures are the hindered phenols, thiosynergists, and hindered amine stabilizers (the latter denoted as HALS or HAS; Hsuan and Koerner, 1998). HAS is an umbrella acronym covering a family of different chemicals with different molecular weights and functions. Thus, the HAS used in the geomembranes discussed in this paper may be quite different to those used in other geomembranes and one cannot generalize conclusions reached in this paper regarding the role of HAS to other geomembranes without specific testing. Much of the research conducted on HAS has been for thin films where the movement of high molecular weight (HMW) HAS from the core to the surface is far more readily achieved than it is in 1.5–2.5 mm thick geomembranes. Thus, there is conflicting evidence in the literature regarding the usefulness of HAS in protecting geomembranes not subject to prolonged sun exposure. For example, Rowe and Shoaib (2017) reported that the time to nominal failure was reached before the AO-S detected by HP-OIT had depleted to a residual value. Thus the 3-stage model based on HP-OIT (Fig. 1) did not apply for that GMB suggesting that the mobile AO-S detected by HP-OIT (i.e., those which deplete which can include low molecular weight HAS) were ineffective at preventing the onset of degradation. This paper will explore the potential effectiveness of the HAS in the four GMBs examined.

1.2. PE-RT geomembranes; recent work

Although several PE-RT studies exist in the plastic pipe literature, GMBs are produced differently and use different additive packages compared to those in plastic pipes and there is a paucity of long-term data on PE-RT GMBs. At high temperatures, PE GMBs experience: (1) material softening (and problems with strength and creep), and (2) rapid depletion of the protective AO-S via leaching, leaving the resulting GMB vulnerable to thermo-oxidative degradation (Scheirs, 2009). Thus, a good HDPE GMB for hot applications is likely one formulated with both a PE-RT grade resin and an AO-S package that is well retained but still active at elevated temperatures, specifically in hot fluids.

In a series of conference papers, Mills and Beaumier (2017); Mills et al. (2019) and Rangel et al. (2017) examined two such PE-RT GMBs aged in air, brine, and chlorinated water between 50 and 110 °C for 1 year reporting that one of the PE-RT GMBs showed notably better Std-OIT retention (than the control HDPE GMB) while the other was only marginally better, however, those studies were not run long enough to understand the HP-OIT depletion (despite the likelihood that HAS were involved). Most recently, Clinton and Rowe (2023) reported a much longer 7.5-year study examining the AO-S depletion of four 1.5-mm HDPE GMBs [two of which were formulated for high temperature and used PE-RT resins] by aging them in synthetic municipal solid waste (MSW) leachate and monitoring their Std- and HP-OIT depletion. It was found that: (1) Although both PE-RT GMBs showed excellent AO-S retention at 85 °C in air (compared to the control GMBs), only one of them showed good AO-S retention in synthetic MSW leachate at the same temperature; (2) the Std- and HP-OIT had notably different times to reach a residual value at the same immersion temperature, and; (3) the AO-S depletion rate appeared more influenced by the nature of the additive package (and its interaction with the leachate e.g., hydrolysis susceptibility) than the resin. However, to date, none of the published studies on PE-RT GMBs have examined the change in their mechanical

Table 1
Initial properties of the GMBs examined.

Property	GMB1	GMB2	GMB3	GMB4
Designator	yF1	yF2	yF3	yF4
Type based on ASTM D883-11	HDPE	HDPE	HDPE	HDPE
PE-RT resin[a]	No	No	Yes	Yes
Production date[b]	2013	2013	2013	2014
Nominal thickness (mm) - (ASTM D5199)	1.5	1.5	1.5	1.5
Color	Black	Black	Black	Black
Resin Density[a] (g/cm^3)	0.937	0.936	0.933	0.939
GMB density[a] (g/cm^3)	0.943	0.945	0.943	0.949
Carbon black[a] (%)	2.4	2.7	2.3	2.3
Std-OIT[c] (min) - (ASTM D3895)	179 ± 2	206 ± 2	209 ± 28	254 ± 16
HP-OIT[c] (min) - (ASTM D5885)	1220 ± 60	950 ± 20	1260 ± 90	1410 ± 70
HLMI (g/10 min) - (21.6 kg)	11.8 ± 0.2	10.2 ± 0.2	19.8 ± 0.3	32.4 ± 0.2
LLMI (g/10 min) - (2.16 kg)	0.096 ± 0.001	0.084 ± 0.002	0.74 ± 0.044	0.57 ± 0.07
Melt flow ratio (–)	123 ± 3	121 ± 5	27 ± 2	56 ± 7
SCR_o[b] (hours) - (ASTM D5397)	7600 ± 1900	8100 ± 300	6500 ± 2250	2800 ± 400
SCR_m[d] (hours) - (ASTM D5397)	2070 ± 310	1370 ± 420	1010 ± 190	650 ± 140
Tensile Properties - (ASTM D6693)	Cross machine direction (XMD)			
Yield Strength (kN/m) Type (IV) size	30.4 ± 1.1	29.2 ± 1.7	27.3 ± 0.7	33.1 ± 0.4
Yield Strain (%)	17.8 ± 0.8	17.6 ± 0.4	20.3 ± 0.4	19.1 ± 0.3
Break Strength (kN/m)	62.4 ± 0.9	60 ± 1.1	58.9 ± 1.5	46.8 ± 2.8
Break Strain (%)	994 ± 16	926 ± 15	960 ± 10	680 ± 32
Break Strength (kN/m) Type (V) size	64 ± 2	63 ± 1	59 ± 2	51 ± 4
Break Strain (%)	790 ± 16	760 ± 19	770 ± 12	580 ± 31

The values in the table represent the mean ± standard deviation.
The GMB properties may vary with time when stored on a roll at room temperature for a long period. In this paper, the terms unaged and initial value correspond to the GMBs just prior to testing commencement.
[a] Provided by GMB manufacturer.
[b] Testing commenced in 2013 (for GMBs 1, 2 and 3) and 2016 (for GMB4). Some SCR rounded to 3 significant digits.
[c] From Clinton and Rowe (2023).
[d] Based on 65 & 75 °C data.

properties with aging, in particular, their durability after the AO-S deplete.

1.3. Objectives

The objectives of this study are to follow on from the study of AO-S depletion reported by Clinton and Rowe (2023) by, for the same GMBs: (a) reporting the changes in the physical-mechanical properties of PE-RT GMB immersed in leachate; and assess the lengths of Stages II and III and the time to nominal failure, t_{NF}; (b) comparing the performance of the PE-RT GMBs with that of two HDPE GMBs using more standard resins; (c) assessing if the 3-stage degradation model applies to Std- and HP-OIT for the four GMBs examined and, lastly; (d) utilizing Arrhenius modelling to predict the time to nominal failure at a range of temperatures.

2. Materials and methods

2.1. Exposure conditions

Accelerated aging was performed by immersing 190 × 100 mm coupons of GMB in 4 L glass jars filled with a synthetic MSW leachate (denoted simply as "leachate" herein) and incubated at 95, 85, 75, 65, and 40 °C (Clinton and Rowe 2023). The synthetic leachate used was a mixture of reverse osmosis (RO) water, organic/inorganic salts, trace metals, surfactant and was reduced (target Eh = -120 mV) to minimize available dissolved oxygen thereby simulating anaerobic leachate found in MSW landfills (e.g., the Keele Valley landfill in southern Ontario, Canada; Rowe et al., 2008). Complete details of this leachate can be found in Rowe et al. (2010a).

2.2. Index testing

The geomembranes were sampled periodically and the change in the physical and mechanical properties was monitored using the melt index test (MI; 190 °C, 21.6 kg; ASTM, 2013b), tensile break properties (ASTM, 2004; type V sized dog-bone specimens), and stress crack resistance (SCR) using the single-point notched constant tensile load test (SP-NCTL; ASTM, 2007). The SCR specimens were examined under a microscope after failure to confirm brittle detachment (i.e., fibril structure).

2.3. HDPE geomembranes examined

Four 1.5-mm HDPE GMBs from the same manufacturer were examined (Table 1). GMB1 was a standard HDPE product with a conventional AO-S package in a medium-density PE (MDPE) resin. GMB2 used a different additive package (e.g., higher carbon black; Table 1) in a standard, although different, MDPE resin. GMB3 and GMB4 had different high-temperature enhanced AO-S packages in different PE-RT resins. All four resins had density within ASTM (2012) medium-density range but with the addition of 2–3% carbon black the GMB density of all four GMBs was within the high-density polyethylene range.

Although GMB1 and 2 used different resins, their physio-mechanical properties were relatively similar (e.g., HLMI, MFR, resin density, tensile yield and tensile break; Table 1) in contrast to their additive packages, which were more different (e.g., Std-OIT, HP-OIT and carbon black content; Table 1). GMB3 and 4 had both dissimilar physio-mechanical properties and AO-S packages. All GMBs had off the roll SCR_o substantially greater than the 500-h required by GRI-GM13 (2021). For instance, GMB2 (SCR_o = 8100 h ± 300 h) took nearly one year to fail in the SP-NCTL test.

3. Results and discussion

3.1. Melt flow index

The high load melt index test ("MI" herein) results (Fig. 2) were used to infer changes in the polymer's molecular weight with aging and to provide insight into the degradation mechanism(s) involved. An

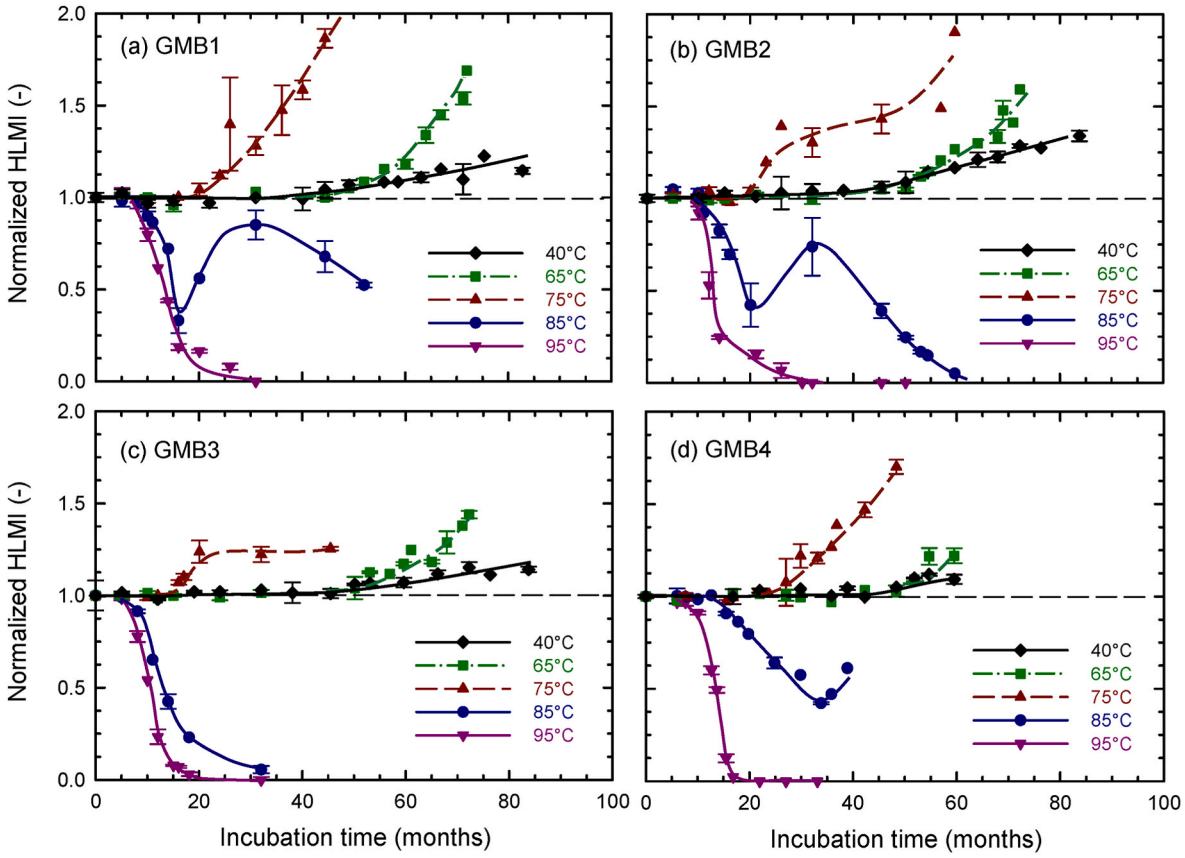

Fig. 2. Change in normalized high load melt index (MI_t/MI_o) with time in leachate at 40, 65, 75, 85 and 95 °C for: (a) GMB1; (b) GMB2; (c) GMB3; and (d) GMB4. 84 months of data was available for GMBs 1, 2 and 3 while 60 months was available for GMB4. Error bars represent the range of duplicate tests.

increase in MI may occur for at least two reasons.

First, as the polymer ages physically prior to oxidative degradation, the chain entanglements in the amorphous zone can slowly disentangle causing a decrease in melt viscosity and increase in MI value (Rudin and Schreiber, 1960). At 40 °C the MI of all four GMBs remained essentially unchanged during the first 40 months of incubation and then gradually started to increase (Fig. 2), however, since there was no evidence of oxidative degradation in the tensile break properties or SCR (discussed later), these gradual MI increases at 40 °C were attributed to chain disentanglement rather than chain scission. Ewais and Rowe (2014) reported a similar finding for a GMB aged in leachate at 40 °C noting that the surfactant present in the leachate (a known plasticizer to PE) likely aided in the chain disentanglement by weakening the interlamellar connections.

Second, chain scission reactions (e.g., from oxidative degradation) are often implied by an increase in MI while cross-linking reactions (typ. Thermal ageing) are often implied by a decrease in MI (Hsuan and Koerner, 1998).

Since the gradual increases at 40 °C were purely morphological (not degradation), this temperature served as a useful reference for assessing the MI time of departure (MI t_{dpr}) at the other incubation temperatures (≥65 °C; Stage I + II; established based on Fig. 2 and given in Table 2) who's departure away from the 40 °C data was associated with polymer degradation (i.e., chain scission or cross-linking). Although the MI, when combined with mechanical data (e.g., tensile break strength/strain or SCR) is a useful indicator of the degradation process involved, it is not used to define nominal failure.

3.2. Tensile break properties

Compared to MI, the change in tensile break strengths (F_b; Fig. 3) and break strains (ε_b; Fig. 4) with time showed more variability, especially just prior to and following the initiation of tensile degradation which made interpreting a single time of departure (t_{dpr}) more difficult than MI (e.g., GMB1-F_b 65 °C; Fig. 3a). However, since the 40 °C data for each GMB was: (a) scattered around the initial value for the duration of the study (it was in Stage I) and; (b) comprised a much larger data set (e.g., n = 61; GMB1 40 °C) compared to the sample size used to establish the initial "off the roll" tensile break values (n = 10), the 40 °C tensile break data could be useful in quantifying the inherent tensile break variability for each GMB and hence help to interpret t_{dpr} at the other temperatures. A decrease exceeding two standard deviations (2 SD) below the mean of a GMB's aged 40 °C dataset (i.e., less than 97.5% of 40 °C data; see dotted lines in Figs. 3 and 4) was used as the criterion to judge the tensile time of departure (t_{dpr}) at the other temperatures. Thus, unlike the t_{dpr} for MI, which was more distinct, the t_{dpr} for tensile break (end of Stage II) for a given GMB at a given ageing temperature occurred over a non-trivial range. For instance, the t_{dpr} for tensile break of GMB1 at 65 °C ranged over almost 2 years from 56 to 77 months (Fig. 3a). The shaded "departure envelopes" at 65 and 75 °C illustrates this range. Thus, there were two ways to define t_{dpr} for tensile break: (a) first departure exceeding 2 SD below the mean of 40 °C data, $t_{dpr\text{-}min}$ and its associated $t_{NF\text{-}min}$ based on the left-hand side of the envelope or; (b) average "best fit" departure, $t_{dpr\text{-}avg.}$ and associated $t_{NF\text{-}avg}$. However, since $t_{dpr\text{-}min}$ represents the conservative assumption, the focus of tensile break

Table 2
Key experimental observations (months).

		Stage I[a]		Stage I+II				Stage I+II+III	
				MI t_{dpr}	Tensile t_{dpr}		SCR t_{dpr}	$t_{NF\ SCR}$	
	T (°C)	Std-OIT	HP-OIT	–	F_b	ε_b	–	A	B
GMB-1	95	1.9	8	8	10	10	11	12	17
	85	2.5	7.2	9.5	11	13	10	12	14
	75	3.4	16	19	24	25	20	23	25
	65	12	48	53	55	56	54	60	72
GMB-2	95	1.9	11	9	13	13	12	13	16
	85	2.6	7.5	10	10	16	10	12.5	14
	75	4.1	17	21	25	37[b]	20	24	27
	65	18	50	56	66	80	56	62	68
GMB-3	95	3.4	5.6	6	8	10	8	9[c]	14[c]
	85	2.5	5.0	7	11	13	7.5	8.5	10
	75	4.2	8.5	14	18	20	13	15	17
	65	15	28	50	72	77	50	53	61
GMB-4	95	6.0	11	10	10	13	13	15	15
	85	5.1	13.5	14	18	22	13.5	14.5	15
	75	13	23	25	30	27	24	26	27
	65	24	48	53	>60	>60	52	60	62

Notes:
1) Time of departure, t_{dpr} (Stage I + II) for MI defined as a departure from the reference temperature (40 °C). t_{dpr} for SCR defined as a departure from the SCR_m plateau.
2) Tensile break t_{dpr} (Stage I + II) is defined as the earliest departure in the tensile failure envelope.
3) SCR t_{NF} is defined two ways: Definition A ($SCR_{NF} = 0.5 \times SCR_m$) and B ($SCR_{NF} = 250$ h). This study focuses on Definition B.
F_b = tensile break strength.
ε_b = tensile break strain.
[a] Stage I data reported by Clinton and Rowe (2023).
[b] Average of two possible departures at 25 and 50 months.
[c] Further reduced to ~180 h and remained there for duration of the study while the other GMBs degraded to ~ zero SCR.

properties for the remainder of this paper is on $t_{dpr\text{-}min}$ (simply termed "tensile t_{dpr}" herein and listed in Table 2; Complete details in supplemental materials Table S1). In summary, the MI was able to detect polymeric changes sooner than tensile break strength or strain for all four GMBs (to varying degrees) *even* when considering the lower bound, earliest observed tensile departure (Table 2). Furthermore, the aged tensile break data was considerably more scattered and hence more difficult to interpret than MI revealing a subtle difference in how the GMB test used affected the inference of the onset of degradation for these GMBs. More importantly, however, the break strains associated with the uni-axial tensile test (>500% break strain; Table 1) do not really reflect the long-term failure mechanism of HDPE GMBs as landfill bottom liners (stress cracking at small, sustained strains). Thus, a more critical property is considered to be SCR.

3.3. Stress-crack resistance and SCR_m

For all GMBs at all temperatures examined (except 40 °C), the SCR decreased significantly within the first 10 months from initially high SCR_o values to lower values that remained stable for a period of time, most notably at 65 and 75 °C, before decreasing again to essentially zero (Fig. 5). Rowe et al. (2019), who studied the tendency of the as-manufactured, off-the-roll, SCR_o to decrease with time to a stable, more representative value, SCR_m (with $SCR_m < 0.5\ SCR_o$ in most cases they examined), attributed this decrease to a combination of two mechanisms: (1) morphological change (i.e., rearrangement of the semi-crystalline structure), and; (2) relaxation of manufacturing induced residual stresses. They noted that the latter usually dominates over morphological change and the data from this study lends support for their conclusion. For example, the melt index at 40 °C does not begin to increase until about 40 months for GMB1 and 2 and about 45 months for GMB3 and 4 signaling a morphological change being detectable at this time (Fig. 2). However, SCR begins to drop shortly after immersion even at 40 °C and by the time morphological change became evident from MI, the SCR had already decreased to 0.4–0.65 SCR_o implying that the relaxation of manufacturing-induced residual stresses played a more dominant role in the drop than morphological change. This decrease has been shown to occur at room temperature as well as at elevated temperatures. For example, Francey and Rowe (2023) reported that rolls stored inside at room temperature experienced a decrease in SCR/SCR_o to 0.64 in 3 years, and 0.37 in 12 years. Except at very high temperatures (generally >75 °C), a notable decrease in SCR occurs before AO-S depletion and without any evidence of polymer degradation (e.g., in the tensile break properties or MI). As such, Rowe et al. (2019) concluded that defining nominal failure as 0.5 SCR_o would be inappropriate and suggested 0.5 SCR_m as a more logical point to define SCR nominal failure (e.g., Fig. 5d).

Manufacturing-induced residual stresses in polyethylene (PE) products, which can be as high as 20% of the yield strength (Chaoui et al., 1987), are in compression on the outer surface and hence retard crack growth since they oppose the externally applied tensile stress in SCR tests (Xu and Bellehumeur, 2008; Poduška et al., 2016). Although the studies which measured PE residual stresses directly have not examined GMBs (e.g., Poduška et al., 2016 studied PE pipe), the study by Rowe et al. (2019) which examined the SCR behavior of 11 different HDPE GMBs (including both blown film and flat die GMBs) in conjunction with the present study offers compelling evidence that the reduction of SCR_o to SCR_m could be explained by the relaxation of residual stresses (for reasons noted earlier). Therefore, it can be argued that the higher the manufacturing-induced residual stress, the greater the drop in SCR with eventual relaxation of those stresses (and lower ratio of SCR_m/SCR_o) as the GMB tends toward a state of (quasi) equilibrium.

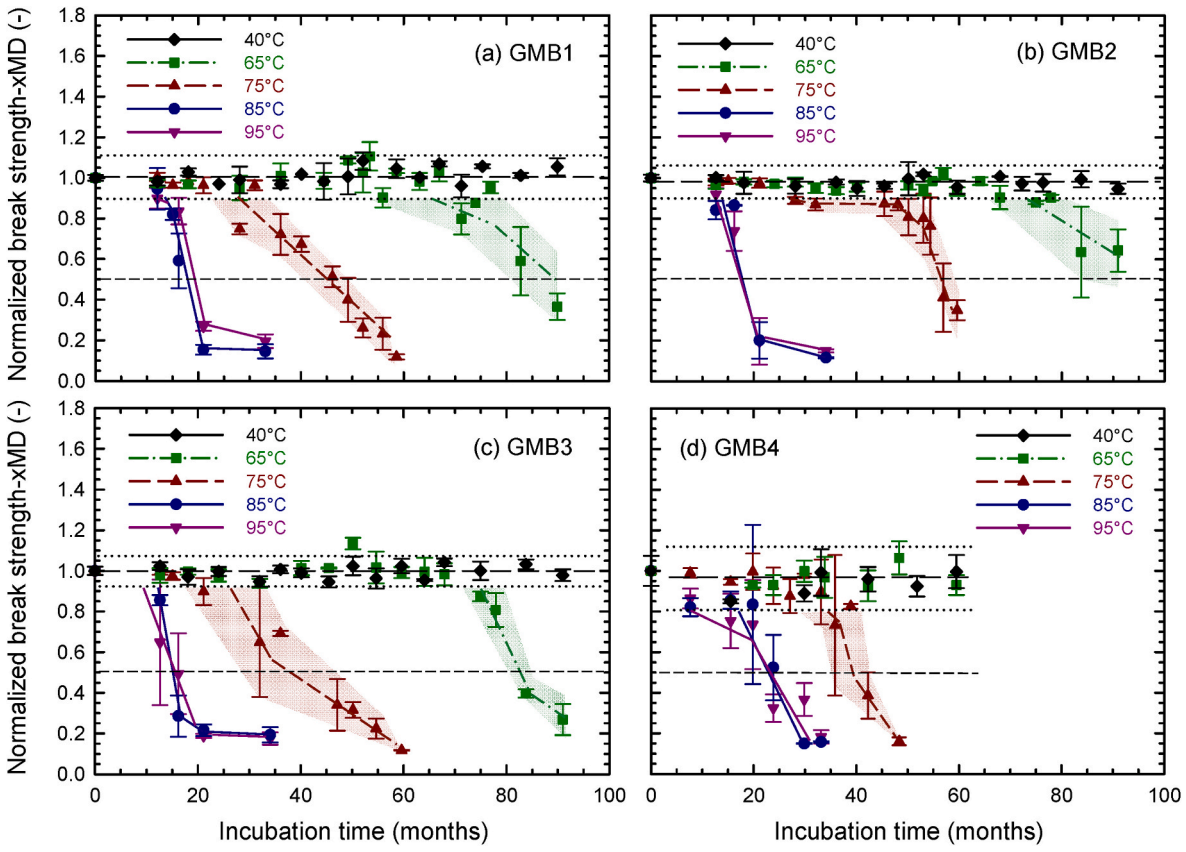

Fig. 3. Change in normalized tensile break strength in the cross-machine direction (F_{bt}/F_{bo}) with time in leachate at 40, 65, 75, 85 and 95 °C for: (a) GMB1; (b) GMB2; (c) GMB3; (d) GMB4. Error bars represent ±1 SD. The middle-dashed line represents mean of 40 °C aged data; Dotted lines represent the upper and lower bounds ±2 SD away from the 40 °C mean (95% of 40 °C data). Shaded "departure envelopes" at 65 and 75 °C illustrate bounds of sample variability after departing the lower 40 °C bound and include a best-fit line.

Results from the present study (up to 90 months) showed that SCR_m was not affected by ageing temperature below about 80 °C (Fig. 5). For example, there was no statistically significant difference between stabilized SCR_m data at 65 and 75 °C for each GMB (at 95% confidence level; Table 3) and at 40 °C, GMB1 and GMB2 started to approach the 65-75 °C SCR_m value by 80 mo (Fig. 5a and b). This suggests that the temperature-dependent SCR_m behavior reported by Ewais and Rowe (2014), who found 25–40 °C SCR_m estimates were higher than those from 55 to 75 °C (for the GMB they examined), was likely a result of their relatively shorter 40-month monitoring period which supports their suspicion that more time may have been needed for SCR to fully stabilize at 25 and 40 °C. Morsy and Rowe (2020), who examined a textured HDPE GMB and its smooth edge, reported no significant difference between stabilized SCR_m at 55 and 75 °C and while their 85 °C results possibly showed a brief SCR_m-like plateau (similar to GMB4; Fig. 5d), it was so fleeting that it could not reliably be used to estimate SCR_m. As a result of the difficulty in observing SCR_m from samples aged at 85 °C, the upper-immersion-temperature limit at which one can assess SCR_m is likely to vary from one GMB to another but in this study appeared somewhere between 75 and 85 °C. Therefore, SCR_m for each GMB in this study was taken as the average of stable (i.e., plateaued) SCR data at 65 and 75 °C since 55 °C was not a test temperature and the tests were not run long enough to reach SCR_m at 40 °C.

The observation that 40 °C data for GMB3 (Fig. 5c) was farther from its SCR_m after 90 months than GMB1 and GMB2 could result from: (a) slower relaxation of residual stresses and/or; (b) more spatial variability in residual stresses across the roll or, less likely; (c) that the fully stable SCR_m itself varied more than the other GMBs. Since Rowe et al. (2019) included GMBs 1, 2 and 3 from this study in their 24-month SCR_m study of 11 HDPE GMBs immersed in leachate at 55 °C, it provided additional SCR data for the present study (and could offer insight into GMB3's 40 °C behavior). Using the same SCR_o values as this study, they reported normalized SCR_m, λ (mean ± SD) = SCR_m/SCR_o of 0.42 ± 0.16 for GMB1; 0.17 ± 0.05 for GMB2; and 0.43 ± 0.13 for GMB3 as compared to the values in this study, viz: 0.27 ± 0.04 for GMB1 (1 SD below their mean); 0.17 ± 0.05 for GMB2 (identical) and 0.16 ± 0.03 for GMB3 (nearly 2 SD below their mean). The fact that the SCR_m estimates reported by Rowe et al. (2019) for GMB1 and GMB3 were both higher and, importantly, more scattered (higher SD) than those from this study suggests that the fully stabilized SCR_m of GMB1 and GMB3 was not completely reached in the duration of their 24-mo. study at 55 °C (while it was reached for GMB2). Aged SCR sample variability (SD) was important in this comparison since variability usually reduces substantially once SCR_m is reached (e.g., compare the 40 °C vs 65/75 °C error bars; Fig. 5) which suggests the reason their higher GMB3 estimate also had higher SD (compared to this study) was because it had not completely reached SCR_m (whereas the identical GMB2 estimates in both studies shared the same low SD). The higher sample variability pre-SCR_m could result from variability in the distribution of residual stresses across the roll. For instance, a large spatial variation in the residual stresses in PE products has been shown to result from non-homogeneity in the molten polymer flow (i.e., flow induced) and/or non-uniform cooling during manufacturing (Chaoui et al., 1987; Xu and Bellehumeur, 2008). This, and the fact that GMB3's SCR_m estimate from Rowe et al. (2019) was the farthest above the values in the present study suggests that the reason GMB3 at 40 °C was farther from SCR_m after 90 months (relative to GMB1 and 2) is a reflection of a relatively slower relaxation of residual stress rather than a more variable SCR_m. This is consistent with the understanding that SCR_m is a fundamental property of the resin at the fully relaxed state (Rowe et al., 2019). This, together

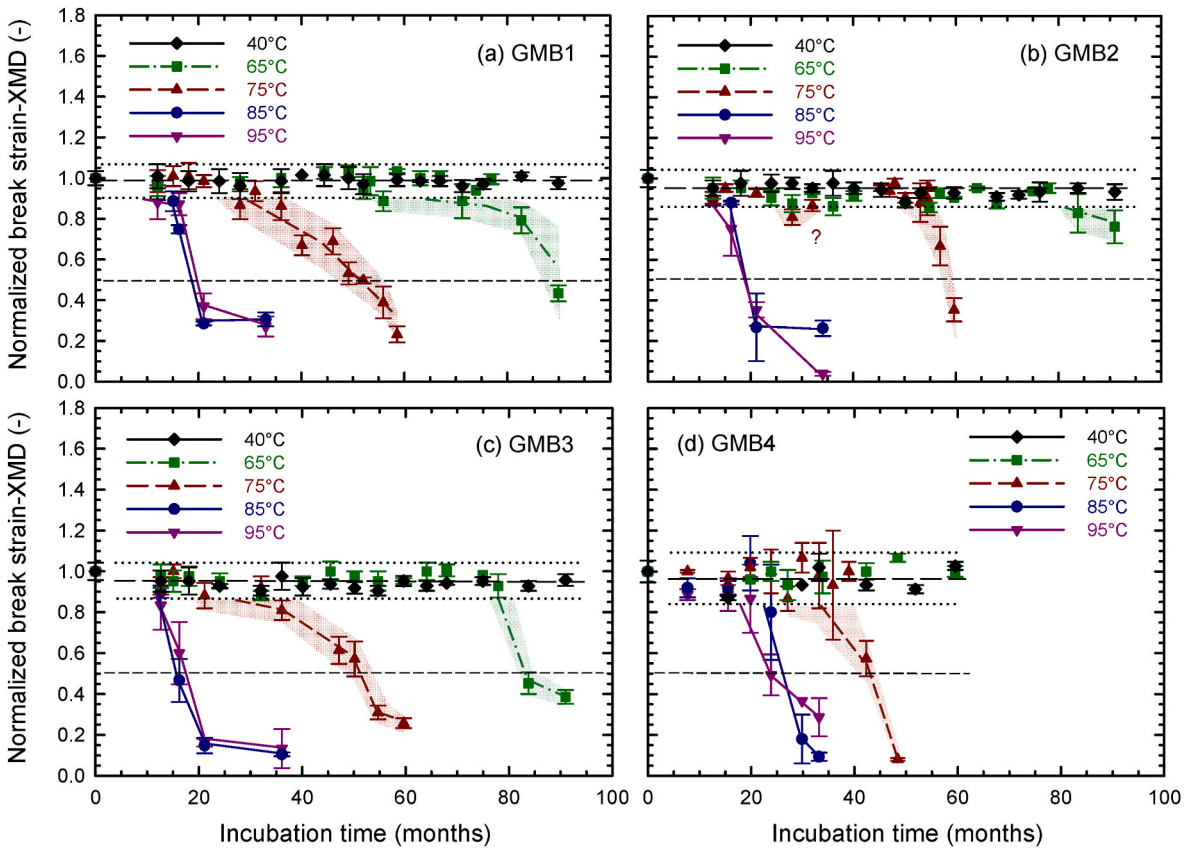

Fig. 4. Change in normalized tensile break strain in the cross-machine direction ($\varepsilon_{bt}/\varepsilon_{bo}$) with time in leachate at 40, 65, 75, 85 and 95 °C for: (a) GMB1; (b) GMB2; (c) GMB3; and (d) GMB4. Error bars represent ±1 SD. The middle-dashed line represents mean of 40 °C aged data; Dotted lines represent the upper and lower bounds ±2 SD away from the 40 °C mean (95% of 40 °C data). Shaded "departure envelopes" at 65 and 75 °C illustrate bounds of sample variability after departing the lower 40 °C bound and include a best-fit line.

with the fact that there was no significant change in melt temperature, lamella thickness, or crystallinity for GMBs 1, 2 and 3 aged at 55 °C in leachate (Morsy 2019) suggests most of the change from SCR_o to SCR_m was due to residual stress relaxation.

Lastly, higher SCR_o did not necessarily result in higher SCR_m (e.g., GMB1 and GMB2; Table 1). Therefore, the only reliable way to know SCR_m is to physically age the GMB; typically, by immersion at about half the melt temperature (Rowe 2020), with immersion at 65–75 °C giving the most reliable estimate in the shortest time possible. Establishing the correct representative SCR of each GMB (SCR_m) was necessary before undertaking the next steps of: (1) identifying SCR t_{dpr}; (2) defining SCR t_{NF} and; (3) predicting SCR t_{NF} at other temperatures.

3.4. Observed SCR time of departure

Since the reduction of SCR_o to SCR_m was not caused by polymer degradation, the time of departure (t_{dpr}) for SCR (i.e., end of Stage II) was taken as a departure from the SCR_m plateau (Fig. 5). The close similarity between the MI and SCR t_{dpr} at the three key observed temperatures (65, 75, 85 °C; Table 2) indicated that this departure from SCR_m was the result of degradation in the polymer back-bone (exception at 95 °C discussed later). At 85 and 75 °C, SCR t_{dpr} was the longest for GMB4, nearly the same for GMBs 1 and 2 and considerably shorter for GMB3 (Table 2). However, at 65 °C $t_{dpr\ SCR}$ for GMB3 (50 mo) was similar to the 54, 56 and 52 mo for GMBs 1, 2 and 4, respectively (Table 2) suggesting a beneficial change in behavior occurred for GMB3 despite its relatively poorer performance at T ≥ 75 °C.

Although the SCR t_{dpr} closely matched the MI t_{dpr} for all four GMBs at 65, 75, and 85 °C, the observed tensile break t_{dpr} at those temperatures was longer for all GMBs (to varying degrees), even when considering the earliest possible tensile departure (Table 2). The near identical t_{dpr} for MI and SCR might have resulted from both index tests measuring the *average* degradation across the GMB thickness (i.e., average of core and surface). In the SCR test (SP-NCTL; ASTM, 2007), the prescribed notch at 20% of the GMB thickness means the crack starts propagating at approximately mid-point between the GMB center (core) and outer surface (Fig. 6) and since the majority of SCR test time occurs near the notch tip (craze accelerates with time), the SP-NCTL test, in effect, focuses on polymer near the mid-point between core and surface. This is actually useful since past GMB studies (Rimal and Rowe 2009; Montes et al., 2012; Abdelaal and Rowe 2014) have shown that degradation does not proceed uniformly throughout the thickness but rather progresses from the surface inwards. Thus, the SCR test's tendency to focus on a depth in-between the extremes of the core and surface can give an average picture of the whole GMB during immersion tests (without being biased to either the core or surface). In the MI test, this "averaging" happens because the GMB sample is shredded and melted at 190 °C so the entire thickness (core and outer surfaces) are completely mixed. The relatively longer tensile break t_{dpr} values compared to those of MI and SCR (Table 2) could imply that the tensile break properties were biased by the core due to the relatively fast nature of the tensile index test that masked the early signs of degradation. For instance, Morsy et al.'s (2021) examination of 12 GMBs in chlorinated water reported that defects in the interlamellar connections associated with oxidative degradation were more evident in the slow NCTL-SCR test than the relatively faster (50 mm/min) tensile test. This delay (lag) in the t_{dpr} for tensile break relative to SCR and fact that the lag varied between the four GMBs (small lag for GMB1; large lag for GMB3) meant that the tensile break properties could not easily be used to predict the SCR t_{dpr}.

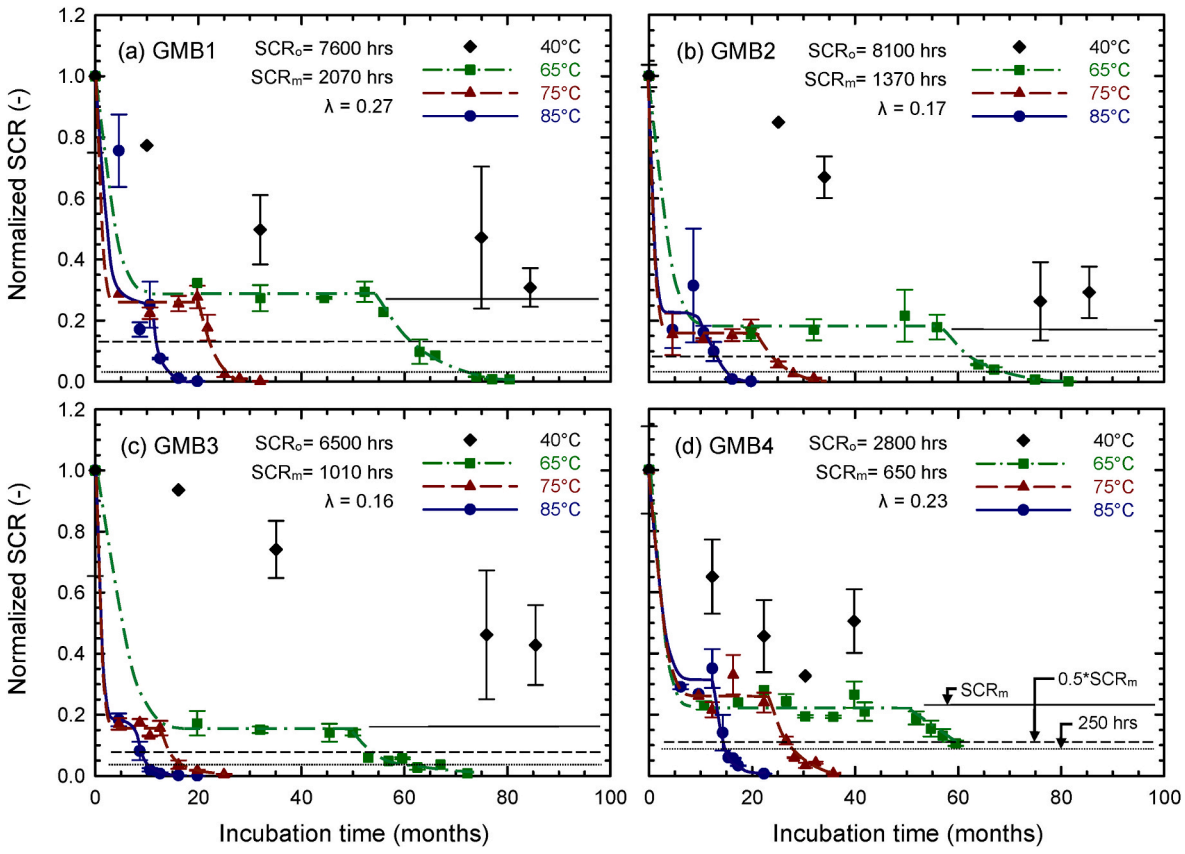

Fig. 5. Change in normalized SCR with incubation time in leachate at 40, 65, 75 and 85 °C [the SCR index test itself runs at 50 °C and is measured in hours] for: (a) GMB1; (b) GMB2; (c) GMB3; and (d) GMB4 (only 60 months data). Error bars for aged values represent range of 2 tests; for initial values they represent the standard deviation of 5 tests. $\lambda = SCR_m/SCR_o$. Two approaches to define the time to nominal failure (t_{NF}) are shown: Method A $SCR_{NF} = 0.5 \times SCR_m$ and Method B $SCR_{NF} = 250$ h.

Table 3
Observed stable SCR_m data (mean ± SD; rounded to 3 significant digits).

	GMB1		GMB2		GMB3		GMB4	
Temperature (°C)	75	65	75	65	75	65	75	65
stable SCR (hours)	1960 ± 290	2200 ± 302	1280 ± 350	1460 ± 480	1030 ± 160	998 ± 220	733 ± 186	612 ± 107
sample size	7	6	8	8	8	8	7	16
different?[a]	no		no		no		no	
combined sample size	13		16		16		23	
SCR_m[b] (hours)	2070 ± 310		1370 ± 420		1010 ± 190		650 ± 141	
λ (−)	0.27 ± 0.04		0.17 ± 0.05		0.16 ± 0.03		0.23 ± 0.05	

Note: $\lambda = SCR_m/SCR_o$.
[a] Statistical significance of 75 and 65 °C difference evaluated using Student's t-test at the 95% confidence level.
[b] Found by pooling stable SCR data at 65 and 75 °C since no significant difference was found between sets.

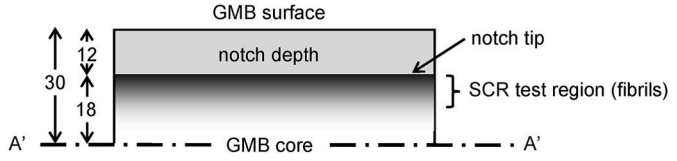

Fig. 6. Half cross-section through a 1.5-mm (60 mil) thick GMB dog bone specimen for SP-NCTL SCR test with notch depth = 0.2 *x* t_{GMB}. Line of symmetry (A′-A′) runs through middle of GMB thickness (core). Vertical dimensions (mil) drawn to scale.

3.5. Issues at 95 °C

Meille et al. (2011) defined annealing as a 'thermal treatment of a solid polymer at a fixed or changing temperature, leading to desirable changes in its physical structure without complete melting' and this change (thickening of lamella crystals) has been shown to have a beneficial effect on slow crack growth (Lu et al., 1992). All four GMBs displayed signs of heat annealing at 95 °C (Supplementary Material Fig. S1), namely: (1) the SCR t_{NF} at 95 °C was either the same or slightly longer than at 85 °C, and; (2) the t_{dpr} for SCR was > t_{dpr} for MI at 95 °C (whereas t_{dpr} for SCR ≈ t_{dpr} for MI at temperatures ≤85 °C; Table 2). Abdelaal et al. (2015) reported a similar case of annealing at 95 °C with retardation in the time at which there was a reduction in SCR that was not observed in the MI. They attributed this to the inability of MI to

Table 4
Observed lengths of Stages II and III based on SCR (months).

GMB	Temperature (°C)	$\Delta t_{II\ Std}$ [a]	$\Delta t_{II\ HP}$ [b]	Δt_{III}	$\Delta t_{II+III\ Std}$ [c]	$\Delta t_{II+III\ HP}$ [d]
1	85	8	3.5	3.5	11	7
	75	17	4.5	5	22	10
	65	42	6	18	60	24
2	85	7.3	2.5	4	11	6.5
	75	16	3	7	23	10
	65	38	6	12	50	18
3	85	5	2.5	2.5	7.5	5
	75	9	5	4	13	9
	65	35	22	11	46	33
4	85	8.5	0	1.5	10	1.5
	75	11	1	3	14	4
	65	28	4	10	38	14

Notes: (1) The length of Stage III (Δt_{III}) is independent of Stage I (independent of OIT test used).
(2) $t_{NF\ SCR}$ defined as the time when SCR depleted to SCR of 250 h.
[a] $\Delta t_{II\ Std} = t_{dpr\ SCR} - t_{I\ Std}$ = length of Stage II (based on Std-OIT).
[b] $\Delta t_{II\ HP} = t_{dpr\ SCR} - t_{I\ HP}$ = length of Stage II (based on HP-OIT).
[c] $\Delta t_{II+III\ Std} = t_{NF\ SCR} - t_{I\ Std}$ = length of Stages II + III (based on Std-OIT).
[d] $\Delta t_{II+III\ HP} = t_{NF\ SCR} - t_{I\ HP}$ = length of Stages II + III (based on HP-OIT).

detect annealing since the MI test erases the effects of annealing during complete melting at 190 °C. Clinton and Rowe (2023), who reported the AO-S depletion of the four GMBs in this study, also reported evidence of annealing at 95 °C. They found the OIT depletion rates at 95 °C deviated from an otherwise linear time-temperature (Arrhenius) relationship at the other temperatures (≤85 °C) which they attributed to annealing after finding annealing associated morphological changes in crystallinity melt scans of the 95 °C aged samples. This agrees with the polyethylene literature showing that annealing can occur at constant elevated temperatures as low as 95 °C (Lu et al., 1992; Meille et al., 2011).

The SCR of specimens aged at 95 °C reached essentially zero SCR (i.e., SCR< 10 h) 1–2 months after specimens aged at 85 °C did for all GMBs except GMB3, which depleted to about SCR = 180 h and remained there for the rest of the study. Although annealing at 95 °C appeared to prevent GMB3 from becoming completely brittle (remaining at SCR = 180 h), it did become completely brittle at T ≤ 85 °C and hence this phenomenon is unlikely to be useful in practice. Ewais and Rowe (2014) reported a similar finding for a leachate immersed GMB where the SCR at 85 °C approached essentially zero while at 95 °C depleted to a residual value of 0.13 SCR_o. Since the 95 °C aged data in this study deviated from the behavior at ≤ 85 °C, it was excluded from Fig. 5 (and the predictive models discussed later) to keep the focus on temperatures ≤85 °C.

3.6. Defining SCR time to nominal failure

In past studies, t_{NF} (i.e., Stage I + II + III) has been defined as the time at which SCR degrades to either 50% of the unaged product (Hsuan and Koerner 1998) or, more commonly, to 50% of the required 500 h specified by GRI-GM13 for new GMBs (GRI-GM13, 2021; Rowe et al., 2009). The former definition (0.5 SCR_o) applied to this study would imply failure at extremely high values (i.e., ~3500 h for GMBs 1, 2 and 3 and ~1400 h for GMB4) well before oxidative degradation occurred. Moreover, in practice few SCR tests are ever run >1000 h and thus, as a result, SCR_o is typically unknown for SCR >1000 h. Morsy and Rowe (2020) proposed an alternative interpretation of t_{NF} as the time when SCR reduces to 50% of SCR_m noting that SCR_m is the more representative long-term value. Thus, one interpretation of t_{NF} was taken as 0.5 SCR_m (Method A; Fig. 5). However, this results in a failure criterion for GMB1 of 1035 h (0.5 × 2070 h; Table 3) which one could argue is unfair since it is greater than the 500-h required by GRI-GM13 (2021) and much greater than GMB4's failure criterion of 325 h (0.5 × 650 h). Therefore, a second interpretation of t_{NF} was taken as 250 h (50% of the minimum required 500 h; Method B; Fig. 5) which permitted equal treatment of each GMB. Since Method B (SCR_{NF} = 250 h) is independent of the GMBs themselves and serves as a useful benchmark for comparing GMBs with significantly different SCR_m, the remainder of this paper focuses on the 250 h SCR failure criterion.

3.7. Observed lengths of stages II and III based on SCR

The observed lengths of Stages II and III based on SCR (Table 4) were deduced from the observed Stage I, Stages I + II (i.e., t_{dpr}) and Stages I + II + III (i.e., t_{NF}). Since Stage II is the induction period between the end of Stage I and the beginning of Stage III, it will vary depending on the OIT test used and thus can be expressed two ways:

$$\Delta t_{II\ Std} = \text{length of Stage II (based on Std-OIT)} = t_{dpr\ SCR} - t_{I\ Std} \quad [1a]$$

$$\Delta t_{II\ HP} = \text{length of Stage II (based on HP-OIT)} = t_{dpr\ SCR} - t_{I\ HP} \quad [1b]$$

The length of Stage III, Δt_{III}, is independent of Stage I and was found by subtracting t_{dpr} from the t_{NF} based on SCR. As an alternative approach, the combined lengths of Stages II + III can be found (independent of t_{dpr}) by subtracting Stage I from the t_{NF} which can be expressed two ways:

$$\Delta t_{II+III\ Std} = \text{length of Stages II + III (based on Std-OIT)} = t_{NF\ SCR} - t_{I\ Std} \quad [2a]$$

$$\Delta t_{II+III\ HP} = \text{length of Stages II + III (based on HP-OIT)} = t_{NF\ SCR} - t_{I\ HP} \quad [2b]$$

The observed Δt_{II} and Δt_{III} both increased with decreasing temperature for all GMBs (Table 4). Since Std-OIT depleted sooner than HP-OIT in the observed temperature range, the observed $\Delta t_{II\ Std} > \Delta t_{II\ HP}$.

With one exception, a Stage II induction period (following the 3-stage conceptual model) was observed for all four GMBs using both Std-OIT and HP-OIT approaches (Table 4). In the exception (GMB4 $\Delta t_{II\ HP}$ at 85 °C), the HP-OIT depletion reached residual at approximately the same time as SCR t_{dpr} resulting in $\Delta t_{II\ HP} \sim 0$ (Supplemental Materials; Fig. S2), however, $\Delta t_{II\ HP} > 0$ at 75 °C (1 mo) and became even longer at 65 °C (4 mo; Table 4). Thus, the 3-stage model still applied to GMB4 despite $\Delta t_{II\ HP}$ ~0 at 85 °C. More extreme cases of the 3-stage model breaking down exist in the literature (where the t_{dpr} occurred well before $t_{I\ HP}$, e.g., see Rowe and Shoaib, 2017; Abdelaal and Rowe, 2014). There are two plausible but competing explanations why the 3-stage model based on HP-OIT can sometimes break down (i.e., $t_{I\ HP} \geq t_{dpr}$): (1) Some of the mobile AO-S detected by HP-OIT (e.g., LMW HAS) were ineffective in the solid-state polymer despite their detection in the melted-state of the 150 °C HP-OIT test under very high oxygen partial pressure. (2) The mobile AO-S detected by HP-OIT had depleted in the outer ~30% of the GMB thickness while there was still some depleting from the core, but since degradation progresses from the surface inwards (and SCR is sensitive to degradation away from core), it only appeared that the 3-stage model broke down on overall measurements even though it was still valid at the outer surfaces of the GMB (i.e., Stage III degradation near the surface while the core is still in Stage I). This is because the SP-NCTL (SCR) test focuses on a more localized region with depth (Fig. 6) whereas the OIT tests used whole thickness specimens. For instance, Montes et al. (2012) examined sections of PE-RT pipe and reported signs of oxidation occurring before OIT depletion but attributed it to the tests themselves since IR spectroscopy (to detect oxidation) used the immediate inner surface of pipe (a few μm) while OIT used 0.2-mm deep samples. It is difficult to tell which of the two competing explanations prevails since both can occur simultaneously for HP-OIT. This is an area where more research is needed.

For all examined GMBs at 85, 75 and 65 °C, $\Delta t_{II+III\ Std} = t_{NF\ SCR} - t_{I\ Std}$ and $\Delta t_{II+III\ HP} = t_{NF\ SCR} - t_{I\ HP}$ can be deduced from the observed $t_{NF\ SCR}$ (Method B), $t_{I\ Std}$ and $t_{I\ HP}$ values given in Table 2. $\Delta t_{II+III\ Std}$ and $\Delta t_{II+III\ HP}$ are important because a correlation can be developed between the rate of antioxidant depletion in jar immersion and the rate in a composite liner system (Sangam and Rowe 2002; Rowe and Rimal 2008a, 2008b; Rowe et al., 2010b) and hence an estimate of the time to failure in a

Table 5
Summary of final predictions (years; rounded to 2 significant digits) (for 5–15 °C see supplementary materials).

									Composite Liner	
T (°C)	GMB	$t_{I\ Std}$	$t_{I\ HP}$	$\Delta t_{II+III\ Std}$	$\Delta t_{II+III\ HP}$	t_{NF} [a]	$t_{NF\ Std}$	$t_{NF\ HP}$	$t_{NF\ Std}$ [b]	$t_{NF\ HP}$ [b]
20	1	460	290	450	55	510	910	340	2000	1000
	2	950	230	250	24	420	1200	260	3500	810
	3	840	130	510	440	670	1300	570	3300	880
	4	590	130	110	530	250	710	660	2100	980
25	1	220	160	250	37	290	470	200	1000	600
	2	420	130	150	17	250	570	150	1600	460
	3	380	75	270	230	360	650	300	1600	480
	4	300	87	72	240	150	380	330	1100	540
30	1	110	95	150	25	170	250	120	510	350
	2	190	78	90	12	140	280	90	750	280
	3	180	45	150	120	190	330	170	750	270
	4	160	57	46	110	94	200	170	580	310
35	1	53	57	85	16	98	140	73	260	210
	2	91	47	56	9	86	150	56	360	170
	3	85	27	82	66	110	170	93	370	160
	4	84	39	30	56	60	110	94	320	190
40	1	27	34	51	11	59	78	45	140	130
	2	44	29	35	6	53	79	36	180	110
	3	41	17	46	36	61	88	53	180	94
	4	46	26	19	28	38	65	54	170	120
45	1	14	21	31	7	36	45	28	80	78
	2	22	18	22	5	32	44	23	97	66
	3	21	10	27	20	35	48	30	98	54
	4	25	18	13	14	25	38	32	98	75
55	1	4.0	8.2	12	3.7	14	16	12	25	32
	2	5.6	7.5	9.3	2.6	13	15	10	28	28
	3	5.5	4.3	9.3	6.8	12	15	11	28	21
	4	8.3	8.8	6.0	3.8	11	14	13	34	34
65	1	1.2	3.3	4.8	1.9	5.6	6.0	5.2	9	13
	2	1.6	3.2	4.2	1.5	5.5	5.7	4.7	10	12
	3	1.6	1.8	3.4	2.4	4.5	5.0	4.2	9	9
	4	2.9	4.5	2.9	1.1	5.0	5.7	5.6	13	16
75	1	0.4	1.5	2.0	1.0	2.4	2.4	2.5	3	6
	2	0.5	1.5	1.9	0.9	2.4	2.4	2.3	3	6
	3	0.5	0.8	1.4	0.9	1.8	1.8	1.7	3	4
	4	1.1	2.4	1.4	0.4	2.4	2.5	2.8	5	9
85	1	0.14	0.68	0.91	0.55	1.1	1.1	1.2	1	3
	2	0.15	0.69	0.94	0.53	1.1	1.1	1.2	1	3
	3	0.16	0.40	0.56	0.37	0.74	0.71	0.76	1	2
	4	0.41	1.3	0.75	0.12	1.2	1.2	1.4	2	5

Notes:
1. All predictions use the 250 h SCR criterion to define nominal failure.
2. The simple t_{NF} [a] predictions are considered the least reliable t_{NF} predictions being only based on 65-75-85 °C data and neglecting the 40 °C Stage I data.
3. All predictions are based on data collected at ≤ 85 °C.
4. Prediction uncertainty increases the farther the temperature is from the temperatures where the data was collected.
$t_{NF\ Std} = t_{I\ Std}$ prediction + $t_{II\ +\ III\ Std}$ prediction [3 ½ temperature model].
$t_{NF\ HP} = t_{I\ HP}$ prediction + $t_{II\ +\ III\ HP}$ prediction [3 ½ temperature model].
$t_{I\ Std}$ and $t_{I\ HP}$ predictions from Clinton and Rowe (2023) [4 temperature model].
[a] Time to nominal failure (t_{NF}) predicted with simple 1/(observed t_{NF}) approach [3 temperature model].
[b] Based on Eq. (3) with $R_a = 3.4$ based on available data and $R_c = 1$ in the absence or data to support a larger value.

composite liner system can be given by the relationship (Rowe et al., 2020):

$$t_{NF\ field} = t_I \times R_a + t_{II+III} \times R_c \quad [3]$$

Where R_a has been established to be ≥ 3.4 based on Std-OIT for T ≤ 40 °C (R_a decreases with temperature to about 3.1 at 55 °C, 2.3 at 75 °C and 1.7 at 85 °C) and R_c is conservatively assumed to be 1. This will be explored later in this paper.

3.8. Prediction of stages II + III and the t_{NF} using arrhenius modelling

Since the study was run for nearly 90 months and the SCR t_{NF} was reached at three useful temperatures for all four GMBs (85, 75, 65 °C; Fig. 5), one relatively simple approach to predict t_{NF} at other temperatures is to construct an Arrhenius plot (i.e., time-temperature relationship) based on the observed t_{NF} values. Because there is no apparent depletion rate, the reciprocal of observed $t_{NF\ SCR}$ (months^{-1}) can be used as the rate in the Arrhenius equation, which can be written as:

$$s_{tNF} = Ae^{-[E_a/(RT)]} \quad [4]$$

where $s_{t\text{-}NF} = 1/t_{NF\ SCR}$, where $t_{NF\ SCR}$ is reported in Table 2 (months^{-1}); E_a = activation energy for $t_{NF\ SCR}$ (J/mol); R = universal gas constant (8.314 J/mol/K); T = absolute temperature (K); and A = constant.

After taking the natural logarithm on both sides of Eq. (4), an Arrhenius plot can be constructed to predict ln ($1/t_{NF\ SCR}$) and hence $t_{NF\ SCR}$ at any temperature. Predictions using this relatively simple approach are given in Table 5.

Using the relatively unsophisticated approach of Eq. (4) to predict t_{NF} at other temperatures, GMBs 1, 2, and 4 performed similarly well and slightly better than GMB3 at the highest temperatures (65–85 °C) while at lower temperatures (e.g., ≤35 °C), GMBs 1, 2 and 3 performed similarly well and better than GMB4 (Table 5; first t_{NF} column). Although the use of Eq. (4) is a valid approach to predict the failure time of GMBs, it does not consider the individual contribution of each stage

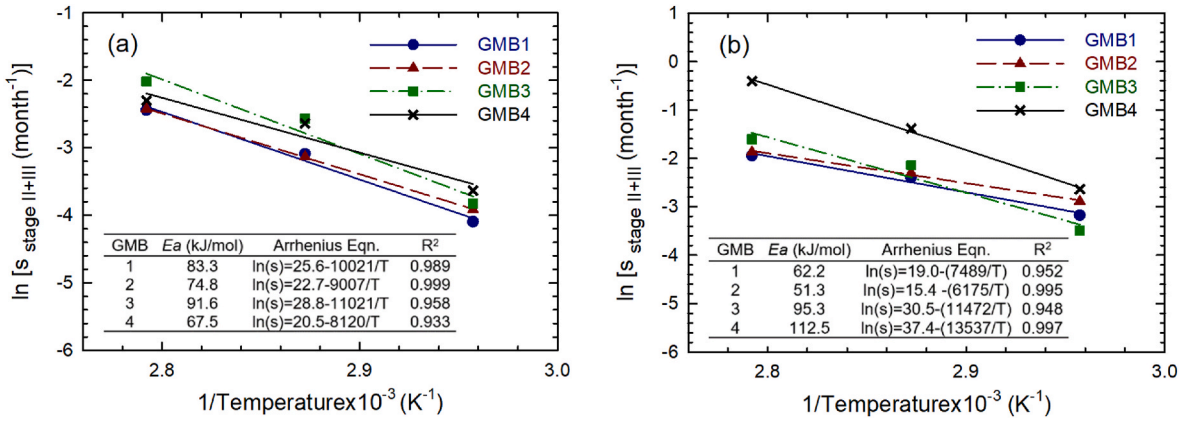

Fig. 7. Arrhenius plots of the observed length of Stage II + III based on SCR data at 85, 75 and 65 °C: (a) $\Delta t_{II+III\ Std}$ and; (b) $\Delta t_{II+III\ HP}$.

since it only relies on the observed t_{NF}. Thus, it completely ignores the Stage I (AO-S depletion) predictions which are considered more credible being based on 4-temperature models (85, 75, 65 and 40 °C) compared to the 3-temperature models (85, 75, 65 °C) of Eq (4) with the observed AO-S depletion rate at 40 °C being important since it is close to real landfill temperatures [it could take a lifetime to observe t_{NF} at 40 °C]. Thus, the more credible Stage I predictions (given in Table 5) are ultimately left unused in the pursuit of t_{NF} if they are not incorporated into the context of nominal failure. One approach to overcome this issue is to construct an Arrhenius plot of the observed combined length of Stages II + III ($\Delta t_{II+III\ Std}$ or $\Delta t_{II+III\ HP}$) and then—using the principal of superposition—add those predictions to the separate Stage I predictions to get the t_{NF}. Such an approach offsets some of the uncertainties of the $t_{NF\ SCR}$ data (3 temperatures) by incorporating the more abundant Stage I data (4 temperatures; including 40 C data). This can be written as (similar to Eq. (3)):

$$t_{NF}\text{ prediction} = t_I\text{ prediction} + t_{II+III}\text{ prediction} \quad [5]$$

To predict the length of Stage II + III, the reciprocal of the observed length $1/(\Delta t_{II+III})$ (month^{-1}) is used as the rate in the Arrhenius equation and since there are two different Stage II lengths ($\Delta t_{II\ Std}$ and $\Delta t_{II\ HP}$), there are two different approaches to find the rate $1/\Delta t_{II+III}$, namely:

$$1/(\Delta t_{II+III\ Std}) = Ae^{-[E_a/(RT)]} \quad [6a]$$

where $\Delta t_{II+III\ Std}$ for Std-OIT is obtained from Table 4; E_a = activation energy of Δt_{II+III} based on Std-OIT (J/mol); R = universal gas constant (8.314 J/mol/K); T = absolute temperature (K); and A = constant; and similarly;

$$1/(\Delta t_{II+III\ HP}) = Ae^{-[E_a/(RT)]} \quad [6b]$$

where $\Delta t_{II+III\ HP}$ for HP-OIT is obtained from Table 4 and other terms are similar to above.

The Arrhenius plots for this approach are shown in Fig. 7. Considering the resulting Stage II+III predictions along with the Stage I predictions (both given in Table 5) for (a) immersed GMB, and (b) a GMB in a composite liner (based on Eq. 3 and listed in Table 5) taken together with Fig. 7, the following observations can be made:

- Different Δt_{II+III} predictions and t_{NF} predictions depended on whether Std-OIT or HP-OIT was used to get t_I.
- $t_{I\ HP} > t_{I\ Std}$ for T ≥ 55 °C. This switched to $t_{I\ HP} < t_{I\ Std}$ around 45–55 °C for GMB2, GMB3 and GMB4 and around 30–35 °C for GMB1.
- $\Delta t_{II+III\ HP} < \Delta t_{II+III\ Std}$ at all temperatures for GMB1, GMB2, GMB3 and for T ≥ 55 °C for GMB4. This only switched to $\Delta t_{II+III\ HP} > \Delta t_{II+III\ Std}$ for GMB4 at T < 45–55 °C.
- In jar immersion, $t_{NF\ HP} > t_{NF\ Std}$ for GMB2 and GMB3 at T > 75 °C, and for GMB1 T ≥ 75 °C, but other than that $t_{NF\ HP} < t_{NF\ Std}$ and the difference increased with decreasing temperature. The only exception was GMB4 where $t_{NF\ Std}$ and $t_{NF\ HP}$ predictions were relatively similar over the full range of temperatures.
- For $\Delta t_{II+III\ Std}$ (Fig. 7a), the activation energy, E_a for each GMB was different but all were within a similar range: GMB1 and GMB3 (83.3 and 91.6 kJ/mol) were marginally higher than GMB2 and GMB4 (74.8 and 67.5 kJ/mol). However, for $\Delta t_{II+III\ HP}$ (Fig. 7b), the E_a of GMB1 and GMB2 (62.1 and 51.3 kJ/mol) were similar but substantially less than GMB3 and GMB4 (95.3 and 112.5 kJ/mol; respectively).
- The higher $\Delta t_{II+III\ HP}$ activation energy (E_a) of the two PE-RT GMBs relative to the more conventional resin GMBs (Fig. 7) implies that GMB4, and to a lesser extent GMB3, require higher thermal energy to degrade than GMB1 and GMB2 after the HP-OIT has depleted to a residual value.
- The benefit of this on predicted $\Delta t_{II+III\ HP}$ for GMB3 and 4 became evident at T < 55 °C [the benefit was likely exaggerated at T < 35 °C due to a combination of being far from the observed range and greater model uncertainty in HP-OIT relative to Std-OIT]. Although this benefit could be attributed to the PE-RT resins, it is noted that all four GMBs: (a) had high residual HP-OIT$_r$ values (Clinton and Rowe, 2023) and; (b) used different AO-S packages and hence one cannot rule out the possibility that GMB3 and GMB4's higher $\Delta t_{II+III\ HP}$ E_a resulted from them using a more efficacious immobile stabilizer than GMB1 and GMB2 (e.g., a more effective HMW HAS type).
- The relative performance of the different GMBs using the superposition approach ($t_{NF\ Std}$ or $t_{NF\ HP}$) differed depending on which OIT test was used. For instance, at 35 °C GMB3 had the longest predicted $t_{NF\ Std}$ (170 y) and GMB4 the shortest (110 y) however, when based on $t_{NF\ HP}$, GMB4 had the longest prediction (94 y) and GMB2 the shortest (56 y).
- Being present in a composite liner rather than immersed [application of Eq (3)] emphasized the difference between $t_{I\ Std}$ and $t_{I\ HP}$ and changed the ranking of the GMBs. Thus, again at 35 °C, GMB3 had the longest predicted for $t_{NF\ Std}$ (370 y) with GMB2 (360 y) and GMB4

Table 6
Arrhenius equations for the four GMBs [ln(s) = a - b/T](T in K).

GMB	$t_{i\ Std}$		$\Delta t_{II+III\ Std}$		$t_{i\ HP}$		$\Delta t_{II+III\ HP}$	
	a[a]	b[a]	a	b	a[a]	b[a]	a	b
1	37	13,090	25.6	10,021	26	9752	19.0	7489
2	40	14,109	22.7	9007	25	9335	15.4	6175
3	39	13,798	28.8	11,021	26	9368	30.5	11,472
4	33	11,747	20.5	8120	19	7457	37.4	13,537

[a] From Clinton and Rowe (2023).

(320 y) being fairly similar but now GMB1 was the shortest (260 y). In all cases below about 55 °C, Std-OIT governed the length of Stage I and dominated the effect on t_{NF}.

- At 55 °C and above, even in a composite liner, the time to nominal failure is 34 years or less with the best performance being from GMB4. Ontario Reg. 232/98 (MoECP 2011) requires that a primary liner have a service life of 150 years in a composite liner. Assuming a typical upper bound temperature for a normal MSW landfill of about 40 °C, this could be achieved by GMBs 2, 3 and 4 and provided it decreases from 40 °C in less than 130 years, the GMB1 would also be adequate.

The "simple" t_{NF} approach of Eqn 4, which can be regarded as OIT-independent (only relying on the observed SCR t_{NF} at 85, 75 and 65 °C) served a useful role knowing that predictions from this approach will tend to *underestimate* both: (a) the real t_{NF} and; (b) approaches that utilize data from a lower temperature (e.g., $t_{NF\ Std}$ and $t_{NF\ HP}$ which utilized 40 °C data). This is because several studies have shown that things are often better (in some cases substantially better) than what was predicted based on data at higher temperatures. For example, Abdelaal et al. (2014) predicted stress cracking failure of a specimen pre-aged to 75 h to be 7 months at 40 °C based on the observed time to stress cracking at 85, 75, 70, 65 and 55 °C; however, after more than 120 months it still has not failed at 40 °C. Thus, the $t_{NF\ HP}$ predictions are suspicious for GMBs 1, 2 and 3 since they were *less* than the simple-t_{NF} predictions (at full range of temperatures) while the $t_{NF\ Std}$ predictions make more sense being greater than simple-t_{NF} approach (three jar immersion t_{NF} columns; Table 5). The only GMB without suspicious $t_{NF\ HP}$ predictions was GMB4 (since both $t_{NF\ HP}$ and $t_{NF\ Std}$ were > simple-t_{NF}). The forgoing shows that $t_{NF\ Std}$ is the most important in any given temperature below 55 °C however one needs to recognize that a geomembrane in a landfill may be exposed to the sun for days to years before it is buried and will not be consistently at one temperature either before or after burial. Thus, both the Std- and HP-OIT packages can both play an important role; which is dominant will depend on the exposure and time-temperature history of the liner. The foregoing statement is not easily visualized simply by inspecting Table 5. However, it can be demonstrated using the time-temperature history for a given landfill. For this purpose, the approach proposed by Rowe and Ewais (2015) for exposed GMBs and Rowe and Islam (2009) for buried GMBs can be used together with the equations in Clinton and Rowe (2023) for OIT depletion rate, s at a given temperature *T*, (Table 6) together with;

$$OIT^*(t) = OIT_k^* \bullet \exp(-s \bullet t) \quad [7]$$

With repeated applications of the equations for $k = 0, 1, \ldots, n$ and $T_o, T_1, \ldots, T_n$ for the sequence of temperatures and length of time at each temperature in the landfill history until time t_i when depletion of the antioxidants is reached. Then for subsequent times, using $\Delta t_{II+III} = 1/s$ at a given temperature T from this paper (Table 6), the proportion of its remaining life (post Stage I) can be calculated. This is best illustrated with an example.

Suppose that GMB4 was buried quickly and then used as a bottom liner in a landfill that initially experienced a rapid increase in temperature to 55 °C where it remained for 30 years, until dropping to 40 °C for 10 years, and finally to 25 °C. Whether GMB4 would be adequate can be assessed by use of the approach described above which, given Table 5, can be simplified as follows.

Considering the Std-OIT approach, the time required for Std-OIT depletion at 55 °C in a composite liner (from $t_{I\ Std}$ in Table 5 and Eq. (3)) is 3.4 × 8.3 = 28 years. Thus, all the antioxidants detected by Std-OIT would be depleted during this 30-year period plus 30–28 = 2 years of the available 6 years (Table 5) in Stage II/III at 55 °C (i.e., 33% of available time in Stages II/III) would be consumed. Dropping to 40 °C there would have been 19 years in Stage II/III of which 33% was consumed by 2 years at 55 °C, leaving 19•(1–0.33) = 12.7 years in Stage II/III remaining of which 10 years would be used leaving 12.7–10 = 2.7 years of time in Stage II/III remaining (i.e., 2.7/19 = 0.14 or 14% of Stage II/III remaining). Finally, dropping to 25 °C, there is 14% of the 72 years (GMB4 $\Delta t_{II+III\ Std}$; Table 5) or 10 years remaining for a total elapsed time to $t_{NF\ Std}$ of 30+10+10 = 50 years.

Considering HP-OIT for the same time-temperature history, the HP-OIT would have just reached residual in the composite liner after 30 years at 55 °C (3.4 × 8.8 = 30 years; Table 5 and Eq (3)). Ten years at 40 °C would consume 10 of the available 28 years (or 10/28 = 36% of the Stages II/III time) leaving 64% of the time in Stages II/III available when the temperature drops to 25 °C, for a remaining 0.64•240 = 154 years. Thus, given this time temperature history, the HP-OIT approach gives a total $t_{NF\ HP}$ = 30+10+154 = 194 years (compared to 50 years for the Std-OIT approach) for GMB4 to reach nominal failure. It would appear that the HAS used to get the HP-OIT values of GMB4 did in fact serve some very useful function in extending the life of the GMB for this time-temperature history. Although the time-temperature history examined here is quite simple, the same approach could be adopted with a more continuous variation in temperature.

The different t_{NF} patterns between lab immersion and a composite liner is a result of the chosen values R_a = 3.4 and R_c = 1. These parameters (R_a being realistic; R_c being conservative) result in more emphasis being placed on Stage I relative to Stage II/III which, for example is why $t_{NF\ HP} > t_{NF\ Std}$ at T > 55 °C in last two columns of Table 5 (it emphasized the longer $t_{I\ HP}$ at T > 55 °C). R_c was conservatively assumed to be 1 however it is expected to be higher in the field and hence even the composite liner values in Table 5 can be regarded as somewhat conservative on this basis, especially for T ≤ 40 °C based on the example given earlier from Abdelaal et al. (2014) in which case it could be argued that R_C » 1 although there is insufficient data to generalize this observation at this time.

4. Practical implications

Although one of the two high-temperature formulated PE-RT GMBs examined had notably (2-fold) longer Std- and HP-OIT depletion in 85 °C leachate relative to the two control HDPE GMBs, its observed time to nominal failure ($t_{NF\ SCR}$) at this temperature was practically the same as the others (15 vs 14 mo). Considering the limitations of making predictions and placing more weight on the actual observations of $t_{NF\ SCR}$ in this 90-month study (i.e., at 65–95 °C; which represents most "hot applications"), the $t_{NF\ SCR}$ of the examined PE-RT GMBs was, at best, only marginally longer than the control HDPE GMBs in the aging conditions examined (constant elevated temperature). However, as illustrated in the previous example, the liner temperature in many practical situations is not constant and the combination of HAS and resins used in the examined PE-RT GMBs could be advantageous in situations where a relatively short period of elevated temperature (that depletes the AO-S) is followed by a reduction in temperature where their relatively long Stage II/III predictions play a useful role.

The foregoing conclusions were based solely on t_{NF} (material resistance to ageing in the absence of tensile strains). However, there may be other aspects of PE-RT GMBs (not tested in the current study) which are beneficial at high temperatures, these can include better short-term material behavior (i.e., stress-strain behavior) and better resistance to material softening and ductile creep at high temperatures. For example, Beaumier et al. (2016) studied the tensile behavior of different GMBs, including PE-RT GMBs, at tensile test temperatures up to 100 °C noting that most PE GMBs soften and lose significant strength and stiffness above ~ 60 °C despite this being well below the melt temperature. They noted that, if loaded in tension, thinning and eventually ductile failure may occur at T > 60 °C, especially on steep side slopes or vertical walls. The PE-RT GMBs they tested, on average, exhibited somewhat better retention of tensile properties at T > 60 °C compared to the control HDPE GMBs they tested (in particular, elastic modulus). This highlights how a PE GMB can fail well before its laboratory derived t_{NF} is reached,

and in the case of hot applications, the vulnerable locations being GMB connections (e.g., to rigid structures) or where it bridges a gap where heat-induced GMB softening could lead to pre-mature failures. Based on the limited available data, it is conceivable that PE-RT could out-perform conventional PE in such locations however more GMB specific research is needed on PE-RT before doing so.

Although Clinton and Rowe (2023) reported substantial AO-S retention of the two PE-RTs (GMB3 and 4) in hot air relative to the control HDPE GMBs, it had no correlation to their depletion in hot leachate and hence the air aging results were misleading. Thus, caution is required when interpreting the results of air aging tests (e.g., GRI-GM13, 2021). Although one important issue with PE GMBs containing hot fluids is the rapid leaching of the protective AO-S, Clinton and Rowe (2023) did not find compelling evidence that PE-RT itself slowed the outward diffusion of AO-S, rather it appeared to be the details of the AO-S package that governed Stage I. Thus, it appears there are two aspects comprising a good "high temperature" GMB: (a) selecting a suitable PE-RT base resin and, arguably more challenging; (b) formulating a masterbatch (i.e., blend of AO-S and other additives) that has good resistance to extraction in hot fluids. For instance, Scheirs (2009) noted that the rapid leaching of AO-S in hot water-immersed GMBs is usually the result of hydrolysis-susceptible AO-S, thus good "high temperature" GMBs will be ones developed with this consideration in mind.

Based on the foregoing discussion and results of this study, it would appear that of the two PE-RT GMBs examined, GMB4 had better overall performance (compared to GMB3) due to it having the best AO-S retention at elevated temperatures while also maintaining a good $t_{NF\ SCR}$. Additionally, given the example in section 3.8, it appeared that the HAS used in GMB4 played a beneficial role in extending its $t_{NF\ SCR}$ for the time-temperature history examined which highlights the importance of considering the anticipated time-temperature history of a containment facility (vs assuming a constant temperature). Lastly, given that annealing can occur at temperatures as low as 95 °C and cause material changes not seen at ≤ 85 °C, immersion test temperatures >85 °C should only be undertaken if the data is needed for applications at these higher temperatures and not for extrapolation to lower temperatures.

5. Summary

The findings for the four geomembranes in the conditions examined are summarized as follows.

1. There was a change in polymer behavior at 95 °C that was not observed at the other temperatures (≤85 °C). Hence, the focus of this study, including the predictive models and conclusions below, is based on the data collected at T ≤ 85 °C.
2. The melt index started to depart at approximately the same time as the stress crack resistance departed from the equilibrium value SCR_m and polymer degradation (Stage III) began to be detected.
3. The tensile break properties were far less sensitive to degradation of the polymer than were the melt index and SCR and hence the time at which Stage II ended for tensile, t_{dpr}, was greater than the t_{dpr} for SCR.
4. The initially high off-the-roll SCR_o of these GMBs (e.g., GMB2 = 8100 h) decreased to a substantially lower but more representative long-term equilibrium value (SCR_m) without any polymer degradation and remained constant for a period of time until the onset of degradation. This was true for both the conventional MDPE and PE-RT resins. This is consistent with previous observations when there has been a significant decrease in SCR attributed to the relaxation of manufacturing-induced residual stresses and morphological change. There was no correlation between SCR_o and SCR_m.
5. Immersion at 65 and 75 °C gave fully stabilized SCR_m values much faster than at 55 °C however SCR_m can be missed at T > 75 °C. Thus, immersing in a fluid of interest between 65 and 75 °C for a few months (or until SCR remains stable) can reveal SCR_m in the shortest time possible.
6. The notably dissimilar times to Std- and HP-OIT depletion ($t_{I\ Std} \neq t_{I\ HP}$) resulted in a significantly different length of Stage II ($\Delta t_{II\ Std}$ and $\Delta t_{II\ HP}$) depending on which OIT test was used.
7. The length of Stage I based on either Std- or HP-OIT was less than the observed $t_{dpr\ SCR}$ (i.e., $[t_{I\ Std}, t_{I\ HP}] < t_{dpr}$) and hence the 3-stage degradation model generally worked for both OIT approaches.
8. Immersion of specimens at 40 °C provided valuable OIT depletion rates, s, that allowed Stage I predictions using data from four temperatures. Thus, the Stage I predictions are considered more reliable than those for Stages II + III which were based on data at three temperatures.
9. At higher temperatures (e.g., 85 °C), GMBs 1, 2 and 4 performed similarly well (1.2–1.4 y) and marginally better than GMB3 (0.8 y). At intermediate temperatures (e.g., 55 °C) all four GMBs had similar $t_{NF\ Std}$ (10–13 y) and similar $t_{NF\ HP}$ (14–16 y). t_{NF} increased rapidly as the temperature was lowered.

6. Conclusions

The durability of four 1.5-mm HDPE geomembranes (GMBs) provided by the same manufacturer each using a different resin and additive package was examined. All GMBs met the requirements of GRI-GM13. Two used different PE-RT resins while two used more conventional PE GMB resins. All four resins were medium-density however, after the addition of carbon black, moved into the high-density range (HDPE). Accelerated aging was conducted at 40, 65, 75, 85, and 95 °C by immersing the GMBs in a synthetic MSW leachate containing a surfactant, inorganic salts, and a reducing agent and the change in key properties was monitored for 90-months with a focus on the change in MI, tensile break and SCR to nominal failure. All GMBs were inferred to contain hindered amine stabilizers (HAS) and their observed Std-OIT and HP-OIT depletion times (Stage I) were notably different at the same temperature. Arrhenius modelling was used to predict the time to nominal failure (t_{NF}) based on SCR for a range of temperatures. For the specific GMBs and conditions examined, the following conclusions were reached.

1. All geomembranes, including the two PE-RT geomembranes, experienced a substantial reduction in stress crack resistance from the SCR_o to the equilibrium value SCR_m with $0.16 \leq SCR_m/SCR_o \leq 0.27$. Immersion of the GMBs in leachate at 65 °C provided the best conditions for obtaining a reliable SCR_m in a relatively short time.
2. The time to depletion of AO-S, t_I, varied substantially between those detected by the Std-OIT test and those detected by the HP-OIT test, with the time to depletion being greatest for HP-OIT for T ≥ 65 °C, and least for T < 55 °C. t_I also varied substantially from one GMB to another as a result of the different AO-S used.

Although examining four different resins and AO-S packages makes it difficult to distinguish the role of the AO-S package (particularly the HAS in the package) from that of the resin, the data suggests that.

3. The HAS used in GMB4 served a useful function in extending the life of the GMB in situations such as encountered in landfills where there is a time-temperature history to be accommodated by the GMB.
4. The PE-RT GMBs studied did not have a clearly observable effect in increasing the time to nominal failure, t_{NF}, at elevated temperatures with the difference between the "standard" HDPE GMB and the best PE-RT GMB not being significantly different at temperatures between 65 and 95 °C.

It is acknowledged that this study only examined two PE-RT GMBs and that other PE-RT resins may exhibit a different performance. Also, this study only considered the material's resistance to aging and it is

acknowledged that there are other reported aspects of PE-RT which may be beneficial at elevated temperatures that were not considered in this study. Except for the last two columns of Table 5, all estimates of time to AO-S depletion and t_{NF} are based on the GMBs immersed in an aggressive simulated MSW leachate (with contact on both sides of GMB). When consideration is given to the AO-S depletion in a composite liner, the predicted times increased substantially as illustrated by the last 2 columns in Table 5.

Data availability

Data will be made available on request.

Acknowledgments

The research presented in this paper was supported by the Natural Sciences and Engineering Council of Canada (NSERC) Strategic Grant STPGP 521237–18. The equipment used was provided by funding from the Canada Foundation for Innovation (CFI) and the Government of Ontario's Ministry of Research and Innovation. Dr. M. Shoaib initiated the testing reported herein but all of the results reported were independently verified and additional tests were initiated to fill gaps in Dr. Shoaib's data. Dr. Shoaib's work in maintaining the tests in the beginning is gratefully acknowledged but it is also noted that Dr. Shoaib made no intellectual contribution to the experimental design, interpretation of the data, or writing of this paper and hence is not a co-author.

Notation

AO-S	Antioxidants & Stabilizers
$E_{a\ II+III}$	Activation energy for the combined length of Stage II + III
GMB	Geomembrane
h	Hours
HAS	Hindered amine stabilizers
$HP\text{-}OIT_r$	Residual HP-OIT
LMW	Low molecular wt
MI	Melt index
mo	Months
SCR_o	Initial stress crack resistance
SCR_m	Representative stress crack resistance
SP-NCTL	Single-point notched constant tensile load test
t_{dpr}	Time of departure
t_{NF}	Time to nominal failure
t_I	Length of Stage I based on Std-OIT ($t_{i\ Std}$) or HP-OIT ($t_{i\ HP}$)
Δt_{II}	Length of Stage II based on Std-OIT ($\Delta t_{ii\ Std}$) or HP-OIT ($\Delta t_{ii\ HP}$)
Δt_{III}	Length of Stage III
$\Delta t_{II+III\ Std}$	$\Delta t_{II\ Std} + \Delta t_{III} = t_{NF} - t_{I\ Std}$
$\Delta t_{II+III\ HP}$	$\Delta t_{II\ HP} + \Delta t_{III} = t_{NF} - t_{I\ HP}$
$t_{NF\ Std}$	Time to nominal failure $t_{I\ Std} + \Delta t_{II+III\ Std}$
$t_{NF\ HP}$	Time to nominal failure $t_{I\ HP} + \Delta t_{II+III\ HP}$
t_{dpr_min}	Earliest time of departure for tensile break
t_{NF_min}	Earliest time to nominal failure for tensile break
t_{NF_SCR}	Time to nominal failure for SCR
y	Years
$[\ ]_{Std}$	Based on Std-OIT

Appendix A. Supplementary data

Supplementary data to this article can be found online at https://doi.org/10.1016/j.geotexmem.2023.11.003.

References

Abdelaal, F.B., Rowe, R.K., Hsuan, Y.G., Awad, R., 2015. Effect of high temperatures on the physical and mechanical properties of HDPE geomembranes in air Geosynthetics International 22, 3, 2015.

Abdelaal, F.B., Rowe, R.K., Brachman, R.W.I., 2014. Brittle rupture of an aged HDPE geomembrane at local gravel indentations under simulated field conditions. Geosynth. Int. 21 (1), 1–23. https://doi.org/10.1680/gein.13.00031.

Abdelaal, F.B., Morsy, M.S., Rowe, R.K., 2019. Long-term performance of a HDPE geomembrane stabilized with HALS in chlorinated water. Geotext. Geomembranes 47, 815–830.

Abdelaal, F.B., Rowe, R.K., 2014. Effect of high temperatures on antioxidant depletion from different HDPE geomembranes. Geotext. Geomembranes (42), 284–301.

ASTM, 2013a. Standard Test Method for Obtaining Hydrostatic Design Basis for Thermoplastic Pipe Materials or Pressure Design Basis for Thermoplastic Pipe Products. ASTM Standard D2837-13. American Society for Testing and Materials, West Conshohocken, PA.

ASTM, 2012. Standard Terminology Relating to Plastics. American Society for Testing and Materials, West Conshohocken, PA. ASTM standard D883.

ASTM, 2014. Standard Specification for PE-RT Plastic Hot and Cold Water Tubing and Distribution Systems. ASTM Standard F2769-14. American Society for Testing and Materials, West Conshohocken, PA.

ASTM, 2004. Standard Test Method for Determining Tensile Properties of Nonreinforced Polyethylene and Nonreinforced Flexible Polypropylene Geomembranes. American Society for Testing and Materials, West Conshohocken, PA. ASTM standard D6693.

ASTM, 2007. Standard Test Method for Evaluation of Stress Crack Resistance of Polyolefin Geomembranes Using Notched Constant Tensile Load Test. ASTM standard D5397. American Society for Testing and Materials, West Conshohocken, PA.

ASTM, 2013b. Standard Test Method for Melt Flow Rates of Thermoplastics by Extrusion Plastometer. American Society for Testing and Materials, West Conshohocken, PA. ASTM standard D1238.

Beaumier, D., Mills, A., Dolez, P., Blond, E., 2016. Tensile resistance of geomembranes for high temperature applications. In: Proceedings of the 69th Canadian Geotechnical Conference. GeoVancouver 2016.

Chaoui, K., Chudnovsky, A., Moet, A., 1987. Effect of residual stress on crack propagation in MDPE pipes. J. Mater. Sci. 22 (11), 3873–3879.

Clinton, M., Rowe, R.K., 2023. Antioxidant-stabilizer depletion of 4 HDPE geomembranes with high HP-OIT in MSW leachate. Geosynth. Int.

Damen, J., Schramm, D., Quack, W., Shenanobish, K., Cham, P.M., 2001. PE-RT, a new class of polyethylene for hot water pipes. In: Proceedings of Plastics Pipes XI. Munich, Germany. Pg. 775-785.

DIN, 2001. Polyethylene Pipes of Raised Temperature Resistance (Germany). – General Quality Requirements, Testing, 16833.

Eldesouky, H.M.G., Brachman, R.W.I., 2018. Calculating local geomembrane strains from a single gravel particle with thin plate theory. Geotext. Geomembranes 46 (1), 101–110.

Ewais, A.M.R., Rowe, R.K., 2014. Effect of aging on the stress crack resistance of an HDPE geomembrane. Polym. Degrad. Stabil. (109), 194–208.

Ewais, A.M.R., Rowe, R.K., Brachman, R.W.I., Arnepalli, D.N., 2014. Service life of a high-density polyethylene geomembrane under simulated landfill conditions at 85 C. J. Geotech. Geoenviron. Eng. 140 (11), 04014060.

Francey, W., Rowe, R.K., 2023. "Long-term stress crack resistance of HDPE fusion seams aged at 85°C in synthetic leachate" can. Geotechnik J accepted 17/8/2022; cgj-2022-0159).

Giroud, J.P., 2016. Leakage control using geomembrane liners. Soils and Rocks 39 (3), 213–235.

GRI-GM13, 2021. Standard Specification for Test Methods, Test Properties, and Testing Frequency for High Density Polyethylene (HDPE) Smooth and Textured Geomembranes: GRI Test Method Geomembrane 13. Revision 16: March 17, 2021. Geosynthetic Research Institute, Folsom, Pa.

Hsuan, Y.G., Koerner, R.M., 1998. Antioxidant depletion lifetime in high density polyethylene geomembranes. J. Geotech. Geoenviron. Eng. 124 (6), 532–541.

ISO 1043-1, 1997. Plastics - Symbols and Abbreviated Terms - Part 1: Basic Polymers and Their Special Characteristics.

Jafari, N.H., Stark, T.D., Rowe, R.K., 2014. Service life of HDPE geomembranes subjected to elevated temperatures. J. Hazardous, Toxic, and Radioact. Waste 18 (1), 16–26.

Leblanc, J., Akbarzadeh, A., Andrews, J., Lu, H., Golding, P., 2011. Heat extraction methods from salinity-gradient solar ponds and introduction of a novel system of heat extraction for improved efficiency. Sol. Energy 85 (No. 12), 3103–3142.

Lu, X., Qian, R., McGhie, A.R., Brown, N., 1992. The effect of annealing on slow crack growth in an ethylene-hexene copolymer. J. Polym. Sci. B Polym. Phys. 30 (No. 8), 899–906.

Marcotte, B.A., Fleming, I.R., 2019. The role of undrained clay soil subgrade properties in controlling deformations in geomembranes. Geotext. Geomembranes 47 (3), 327–335.

McWatters, R.S., Jones, D.D., Rowe, R.K., Markle, J.M., 2020. Investigation of a decommissioned landfill barrier system containing polychlorinated biphenyl (PCB) waste after 25 years in service. Can. Geotech. J. 57 (6), 882–902.

Meille, S.V., Allegra, G., Geil, P.H., He, J., Hess, M., Jin, J., Kratochvil, P., Mormann, W., Stepto, R., 2011. Definitions of terms relating to crystalline polymers (IUPAC recommendations 2011). Pure Appl. Chem. 83 (No. 10), 1831–1871.

Mills, A., Beaumier, D., 2017. Long-Term Performance of HDPE Geomembranes Exposed to High Service Temperature ASCE Geotechnical Frontiers 2017, pp. 22–31. Orlando, Florida.

Mills, A., Fraser, B., Beaumier, D., 2019. Long-term Performance of HDPE Geomembranes Exposed to a High Temperature Brine Solution. IFAI Geosynthetics Conference, Houston, Texas.

Montes, J.C., Cadoux, J., Creus, S., Touzain, E., Gaudichet-Maurin, Correc, O., 2012. Ageing of polyethylene at raised temperature in contact with chlorinated sanitary hot water. Part I—Chemical aspects Polymer Degradation and Stability 97, 149–157.

MoECP, 2011. Ontario Regulation 232/98: Landfilling Sites, Environmental Protection Act, Revised Regulations of Ontario 1990. Government of Ontario. Amendment of October 2011.

Morsy, 2019. Effect of Chemical and Physical Aging on the Longevity of Smooth and Textured Geomembranes in Geoenvironmental Applications. PhD Thesis. Queen's University, Kingston, ON.

Morsy, M.S., Rowe, R.K., 2020. Effect of texturing on the longevity of high-density polyethylene (HDPE) geomembranes in municipal solid waste landfills. Can. Geotech. J. 57.

Morsy, M.S., Rowe, R.K., Abdelaal, F.B., 2021. Longevity of 12 geomembranes in chlorinated water. Can. Geotech. J. 58 (4), 479–495.

Poduška, J., Hutař, P., Kučera, J., Frank, A., Sadílek, J., Pinter, G., Náhlík, L., 2016. Residual stress in polyethylene pipes. Polym. Test. 54, 288–295.

Rangel, E., Mills, A., Beaumier, D., Fraser, B., 2017. A new geomembrane for chlorinated water containment. In: 1st International Conference on Technology and Application of Geosynthetics. Geosynthetics, 2017, Santiago, Chile, pp. 1–8.

Redhead, A., Frank, A., Pinter, G., 2012. Accelerated investigation of the effect of chlorine dioxide on the long-term failure behavior and the material aging of polyethylene for raised temperature resistance. In: Proceedings of Plastic Pipes XVI Conference, pp. 1–10.

Rimal, S., Rowe, R.K., 2009. Diffusion modelling of OIT depletion from HDPE geomembrane in landfill applications. Geosynth. Int. 16 (3), 183–196.

Rowe, R.K., 2011. Systems engineering: the design and operations of municipal solid waste landfills to minimize leakage of contaminants to groundwater. Geosynth. Int. 16 (6), 391–404.

Rowe, R.K., 2020. Protecting the environment with geosynthetics: 53rd karl terzaghi lecture. J. Geotech. Geoenviron. Eng. 146 (9).

Rowe, R.K., Ewais, A.R., 2015. Ageing of exposed geomembranes at locations with different climatological conditions. Can. Geotech. J. 52 (3), 326–343. https://doi.org/10.1139/cgj-2014-0131.

Rowe, R.K., Rimal, S., 2008a. Depletion of antioxidants from an HDPE geomembrane in a composite liner. ASCE J Geotech. Geoenviron. 134 (1), 68–78.

Rowe, R.K., Rimal, S., 2008b. Ageing of HDPE geomembrane in three composite liner configurations. ASCE J Geotech. Geoenviron. 134 (7), 906–916.

Rowe, R.K., Shoaib, M., 2017. Effect of brine on long-term performance of four HDPE geomembranes. Geosynth. Int. 24 (5), 508–523.

Rowe, R.K., Islam, M.Z., 2009. Impact on landfill liner time-temperature history on the service-life of HDPE geomembranes. Waste Manag. 29 (10), 2689–2699.

Rowe, R.K., Islam, Z., Hsuan, Y.G., 2008. Leachate chemical composition effects on OIT depletion in an HDPE geomembrane. Geosynth. Int. 15 (2), 136–151.

Rowe, R.K., Rimal, S., Sangam, H., 2009. Ageing of HDPE geomembrane exposed to air, water and leachate at different temperatures. Geotext. Geomembranes 27 (2), 137–151.

Rowe, R.K., Islam, M.Z., Hsuan, Y.G., 2010a. Effect of thickness on the ageing of HDPE geomembranes. ASCE J Geotech. Geoenviron. 136 (2), 299–309.

Rowe, R.K., Islam, M.Z., Brachman, R.W.I., Arnepalli, D.N., Ewais, A.R., 2010b. Antioxidant depletion from an HDPE geomembrane under simulated landfill conditions. ASCE J Geotech. Geoenviron. 136 (7), 930–939.

Rowe, R.K., Abdelaal, F.B., Islam, M.Z., 2014. Aging of high-density polyethylene geomembranes of three different thicknesses. J. Geotech. Geoenviron. Eng. 140 (5) https://doi.org/10.1061/(ASCE)GT.1943-5606.0001090, 4014005-1 to 4014005-11.

Rowe, R.K., Morsy, M.S., Ewais, A.M.R., 2019. Representative stress crack resistance of polyolefin geomembranes used in waste management. Waste Manag. 100, 18–27. https://doi.org/10.1016/j.wasman.2019.08.028.

Rowe, R.K., Abdelaal, F.B., Zafari, M., Morsy, M.S., Priyanto, D.G., 2020. An approach to geomembrane selection for challenging design requirements. Can. Geotech. J. 57 (10), 1550–1565. https://doi.org/10.1139/cgj-2019-0572.

Rudin, A., Schreiber, H.P., 1960. Time dependence of viscosity in capillary extrusion of polyethylene. J. Polym. Sci. 143, 261–264.

Sangam, H.P., Rowe, R.K., 2002. Effects of exposure conditions on the depletion of antioxidants from HDPE geomembranes. Can. Geotech. J. 39 (6), 1221–1230.

Scheirs, J., 2009. A Guide to Polymeric Geomembranes. Wiley Series in Polymer Science, 978-0-470-51920-2.

Tognon, A.R.M., Rowe, R.K., Brachman, R.W.I., 1999. Evaluation of side wall friction for a buried pipe testing facility. Geotext. Geomembranes 17 (4), 193–212.

Touze, N., 2020. Healing the world: a geosynthetics solution. Geosynth. Int. 1–31.

Xu, H., Bellehumeur, C.T., 2008. Thermal residual stress development for semicrystalline polymers in rotational molding. Polym. Eng. Sci. 48 (2), 283–291.